Research Paper

Identification of prognostic aging-related genes associated with immunosuppression and inflammation in head and neck squamous cell carcinoma

Jing Yang[1,2], Qingshan Jiang[3], Lijun Liu[3], Hong Peng[3], Yaya Wang[3], Shuyan Li[3], Yanhua Tang[3], Jing Yu[3], Runliang Gan[2], Zhifeng Liu[3]

[1]Department of Gastroenterology, The First Affiliated Hospital of University of South China, Hengyang 421001, Hunan Province, P.R. China
[2]Cancer Research Institute, Hunan Province Key Laboratory of Tumor Cellular and Molecular Pathology, University of South China, Hengyang 421001, Hunan Province, P.R. China
[3]Department of Otorhinolaryngology, The First Affiliated Hospital of University of South China, Hengyang 421001, Hunan Province, P.R. China

Correspondence to: Zhifeng Liu, Runliang Gan; **email:** liuzf@usc.edu.cn, ganrunliang@usc.edu.cn
Keywords: head and neck squamous cell carcinoma (HNSCC), aging-related genes (AGs), prognosis, inflammation, immunosuppression
Received: July 21, 2020 **Accepted:** September 29, 2020 **Published:** November 24, 2020

ABSTRACT

Aging is regarded as a dominant risk factor for cancer. Additionally, inflammation and asthenic immune surveillance with aging may facilitate tumor formation and development. However, few studies have comprehensively analyzed the relationship between aging-related genes (AGs) and the prognosis, inflammation and tumor immunity of head and neck squamous cell carcinoma (HNSCC). Here, we initially screened 41 differentially expressed AGs from The Cancer Genome Atlas (TCGA) database. In the training set, a prognosis risk model with seven AGs (APP, CDKN2A, EGFR, HSPD1, IL2RG, PLAU and VEGFA) was constructed and validated in the TCGA test set and the GEO set ($P < 0.05$). Using univariate and multivariate Cox regression analyses, we confirmed that risk score was an independent prognostic factor of HNSCC patients. In addition, a high risk score was significantly correlated with immunosuppression, and high expression of PLAU, APP and EGFR was the main factor. Furthermore, we confirmed that a high risk score was significantly associated with levels of proinflammatory factors (IL-1α, IL-1β, IL-6 and IL-8) in HNSCC samples. Thus, this risk model may serve as a prognostic signature and provide clues for individualized immunotherapy for HNSCC patients.

INTRODUCTION

Head and neck squamous cell carcinoma (HNSCC) ranks sixth among cancer-related deaths, with over 300,000 deaths and 600,000 new cases annually worldwide [1]. The main causes of HNSCC include alcohol consumption, smoking, and high-risk human papillomavirus (HR-HPV) infection [2, 3]. Despite innovations in the multimodal treatment of HNSCC, including surgery, chemoradiotherapy, and targeted drugs, the 5-year survival rate has not improved significantly [4]. Therefore, robust and reliable biomarkers are necessary for efficient early diagnosis and individualized intervention strategies to decrease the mortality rates of HNSCC patients.

Aging is regarded as a time-based or progressive decline of internal physiological function and as a

dominant risk factor for many chronic diseases, including cancer, which is now a hot field of cancer research [5, 6]. Cellular senescence acts as a key contributor to the aging progress and to the development of cancers [7]. The effects of senescent cells on tumors are extremely complex, which can be both profitable and deleterious. The senescent neoplastic cells induced by oncogenesis can cause cell-cycle arrest, which appears to be a puissant anti-tumor mechanism [8]. However, the effect of senescent cells on neighboring cancer cells may be the opposite and is closely associated with the secretion of senescence-associated secretory phenotype (SASP) factors [9–11]. Furthermore, cellular senescence-related inflammation has dual effects on tumor immunity [12–14]. Aging-related genes (AGs) play an important role in the regulation of cellular senescence, which can not only inhibit tumors by regulating tumor cell senescence but also promote the development, invasion, metastasis, progression and poor prognosis of tumor [6, 15–17]. However, few studies have systematically analyzed the relationship between AGs and the prognosis of head and neck squamous cell carcinoma (HNSCC). In addition, their correlations with inflammation and tumor immunity in HNSCC remain unclear.

The human aging genome resource (HAGR) is a database identifying a robust set of aging-specific network characteristics that has revealed aging-related genes as network hubs via systemic analysis of the biology and genetics of the human aging process [18]. To evaluate the prognostic values of AGs in HNSCC, we downloaded gene expression profiles of HNSCC patients from The Cancer Genome Atlas (TCGA) database for risk model construction to reveal the AG set related with the prognosis of HNSCC and the potential association between the risk model and inflammation and tumor immunity.

RESULTS

Analysis of differentially expressed AGs in HNSCC samples

A total of 307 human AGs (Supplementary Table 1) obtained from the HAGR were distributed on all chromosomes, except for sex chromosome Y (Supplementary Figure 1). Based on the expression of the AGs in the TCGA dataset (clinical characteristics are showed in Table 1), we identified 41 differentially expressed AGs (DEAGs), including 39 upregulated and 2 downregulated DEAGs (FDR < 0.05 and |logFC| > 1). The DEAGs are listed in Supplementary Table 2 and are visualized with a hierarchical cluster heat map (Figure 1A) and a volcano plot (Figure 1B).

Functional analysis of DEAGs in the TCGA data set

The potential function and connection of DEAGs in the TCGA dataset were analyzed using GO and KEGG pathway analyses. The top 30 enriched pathways of KEGG pathway analysis are shown as an enriched scatter diagram (Figure 2A). These results revealed that the DEAGs might be associated with cell cycle, cellular senescence, microRNAs in cancer, human T-cell leukemia virus 1 infection and other KEGG pathways in multiple cancers. The top 10 enriched GO terms of BP, CC and MF for the DEAGs are also shown as a scatter diagram (Figure 2B). The most significantly enriched term in the biological process was related to the aging process. These GO terms were also associated with the occurrence and development of cancer. The functional analysis revealed that the DEAGs are closely related to aging, cellular senescence and cancer.

Identification of a prognostic risk model in the TCGA training set

To identify prognostic DEAGs in HNSCC, the expression of the 41 DEAGs from the TCGA training set was assessed by univariate Cox regression analysis. Seven survival-associated DEAGs, including APP, CDKN2A, EGFR, HSPD1, IL2RG, PLAU and VEGFA, in HNSCC are shown by a forest plot (Figure 1C). Then, a prognostic risk model of 7 survival-associated DEAGs was constructed with LASSO regression analysis. The information and the coefficient values of the 7 genes are displayed in Table 2. The prognostic risk score of each patient was calculated with the following formula:

Risk score = APP * 0.0026 + CDKN2A * (-0.0132) + EGFR * 0.0016 + HSPD1 * 0.0048 + IL2RG * (-0.0113) + PLAU * 0.0017 + VEGFA * 0.0215

The patients from the TCGA training set were classified into low-risk and high-risk groups based on the median cutoff value of the risk score (0.709). Survival analysis indicated that the overall survival (OS) of the high-risk group was significantly worse than that of the low-risk group (P < 0.001, Figure 3A). The receiver operating characteristic (ROC) curves analysis demonstrated acceptable discrimination with the area under the ROC (AUC) of 0.664, which was higher than the AUC of other clinical parameters (Figure 3B). The risk plot with the distribution of patients based on risk scores, the survival status of individual HNSCC patients and the heat maps of the expression profiles of the risk genes are displayed in Figure 4A.

Verification of the prognostic risk model in the validation data sets

To validate the robustness of the prognostic risk model of the risk genes, we tested the model with independent validation data sets. With the prognostic risk model from the TCGA training data set, all patients in the TCGA test data set were also classified into high-risk (n = 123) and low-risk (n = 126) groups. Kaplan-Meier survival curve analysis demonstrated patient OS in the low-risk group was better than that in the high-risk group ($P < 0.01$, Figure 3C). ROC curves analysis for the TCGA test set achieved an AUC of 0.608, which was higher than the AUC for the other clinical parameters (Figure 3D).

Further validation of the risk model for prognostic prediction was performed using an external independent GEO data set (GSE65858) with 270 HNSCC patients (clinical characteristics are showed in Table 1). With the same risk model, the patients in the GEO test set were segregated into high-risk (n = 157) and low-risk (n = 113) groups, and the model could distinguish patient survival between the high-risk and low-risk groups ($P < 0.01$, Figure 3E). The ROC curves analysis for the GEO test set achieved an AUC of 0.606, which was higher than the

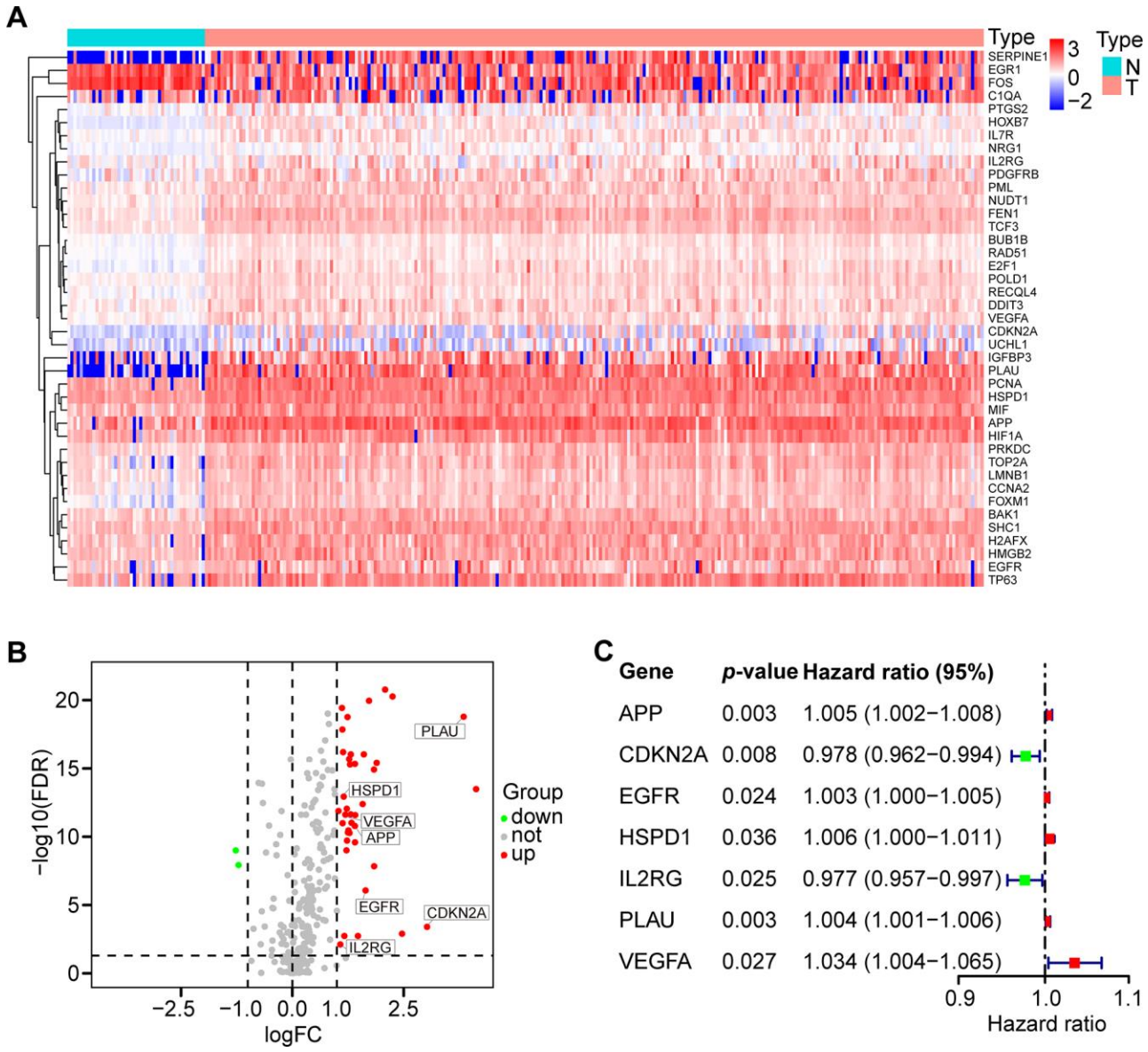

Figure 1. Differential expression of aging-related genes (AGs) and 7 AGs of prognostic risk models in HNSCC samples. (**A**) Hierarchical cluster heat map visualizing 41 differentially expressed AGs (DEAGs). (**B**) Volcano plot showing 39 upregulated and 2 downregulated DEAGs (FDR < 0.05 and |logFC| > 1). (**C**) Forest plot showing the characteristics of 7 risk DEAGs in the prognostic risk models.

AUC of the other clinical parameters, except for T stage (Figure 3F).

A similar analysis was also exploited in the TCGA all data set. The patients in the TCGA all set were divided into high-risk (n = 248) and low-risk (n = 250) groups with significantly different survival ($P < 0.001$, Figure 3G). ROC curves analysis for the TCGA all data set achieved an AUC of 0.632, which was higher than the AUC of the other clinical parameters (Figure 3H).

The risk plot distribution, survival status, and expression of risk genes of the patients in the TCGA and GEO (GSE65858) test sets and TCGA all data set are shown in Figure 4B–4D.

Independent prognostic predictive value of the risk score in HNSCC patients

To investigate the independence of the risk model in clinicopathological factors, we performed univariate and multivariate Cox regression analysis of the clinicopathological parameters of the patients in the TCGA training set, TCGA test set, GEO test set and TCGA all data set, including risk score, age, gender, grade, clinical stage, and TNM stage. Among the training set and multiple test sets, univariate and multivariate Cox regression analyses showed that only the risk score was consistently significantly associated with prognosis, such as the TCGA training set (HR = 3.111, 95% CI = 2.042-4.741, $P < 0.001$; HR = 3.600, 95% CI = 2.293-5.652, $P < 0.001$, respectively, Figure 5A, 5B), the TCGA test set (HR = 1.573, 95% CI = 1.068-2.316, $P < 0.05$; HR = 1.520, 95% CI = 1.027-2.251, $P < 0.05$, respectively, Supplementary Figure 2A, 2B), the GEO data set (HR = 1.239, 95% CI =1.052-1.459, $P < 0.05$; HR = 1.238, 95% CI = 1.045-1.466, $P < 0.05$, respectively, Supplementary Figure 2C, 2D) and the TCGA all data set (HR = 2.148, 95% CI = 1.619-2.850, $P < 0.05$; HR = 2.202, 95% CI = 1.650-2.939, $P < 0.05$, respectively, Supplementary Figure 2E, 2F). The results revealed that the risk model is a robust

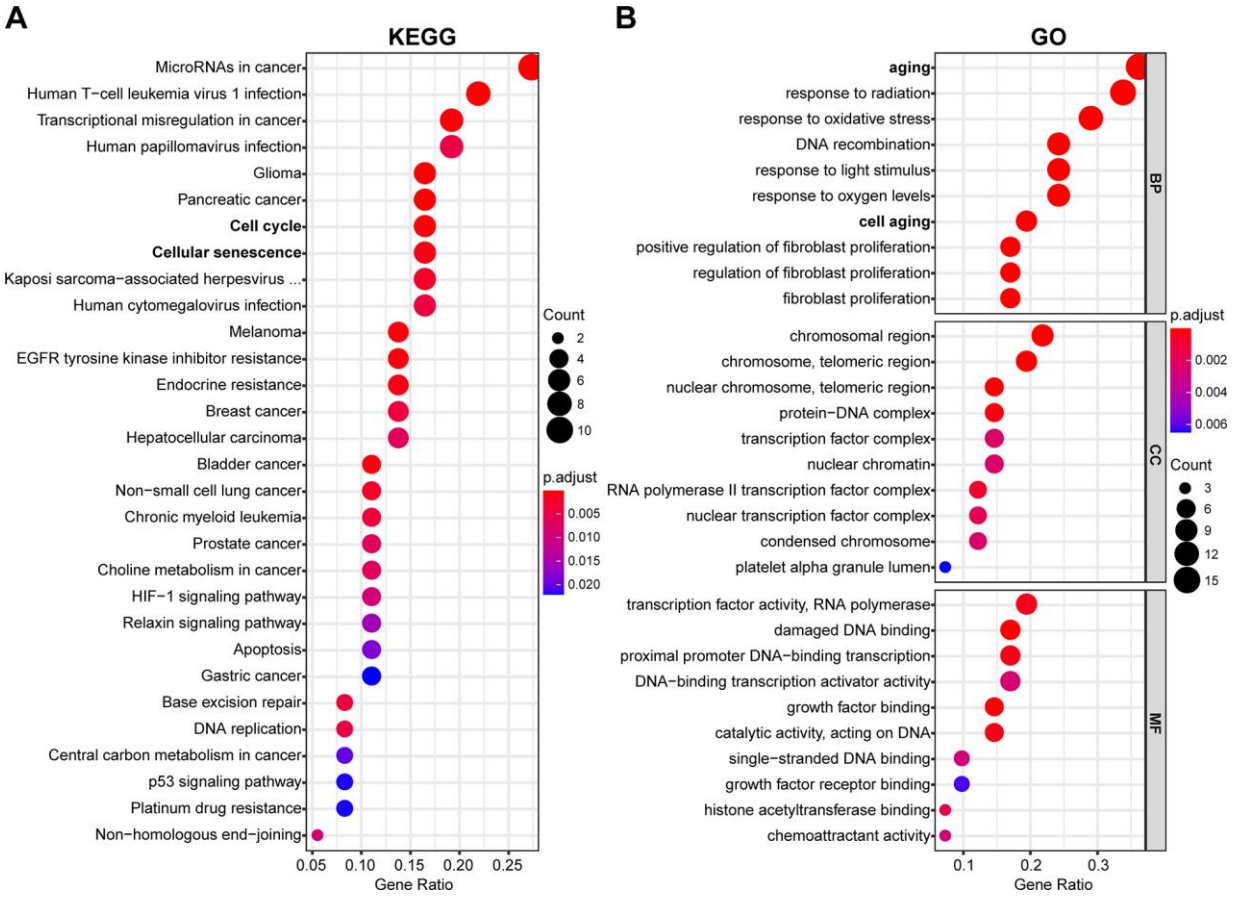

Figure 2. Functional enrichment analysis of DEAGs of the TCGA data set. (**A**) The top 30 enriched pathways from KEGG pathway analysis are displayed using an enriched scatter diagram. (**B**) The top 10 enrichment GO terms of BP, CC and MF for DEAGs are also displayed with a scatter diagram. KEGG, Kyoto Encyclopedia of Genes and Genomes. GO, Gene Ontology; BP, biological process; CC, cell component; MF, molecular function.

Table 1. Clinical characteristics of HNSCC patients in the TCGA and GEO data sets.

Clinical characteristics	TCGA		GEO (GSE65858)	
	n=500	%	n=270	%
Age				
< 60	220	44.0	153	56.7
≥ 60	280	56.0	117	43.3
Gender				
Female	133	26.6	47	17.4
Male	367	73.4	223	82.6
Histologic grade				
G1-2	360	72.0		
G3-4	121	24.2		
Gx	16	3.2		
NA	3	0.6		
Stage				
I-II	114	22.8	55	20.4
III-IV	372	74.4	215	79.6
NA	14	2.8		
T classification				
T1-2	176	35.2	115	42.6
T3-4	309	61.8	155	57.4
Tx	11	2.2		
NA	4	0.8		
N classification				
N0	239	47.8	94	34.8
N+	239	47.8	176	65.2
Nx	18	3.6		
NA	4	0.8		
M classification				
M0	470	94.0	263	97.4
M1	5	1.0	7	2.6
Mx	20	4.0		
NA	5	1.0		
Vital status				
Deceased	218	43.6	94	34.8
Living	282	56.4	176	65.2

prognostic index independent of other clinicopathological parameters.

Association between the risk score and the clinicopathological characteristics of HNSCC patients in the TCGA data set

Next, the association between the risk score and clinicopathological parameters was investigated (Figure 5C–5G, Table 3). The level of risk score was significantly related to histological grade ($P < 0.05$), clinical stage ($P < 0.05$), and T stage ($P < 0.001$). However, it was not correlated with other clinicopathological parameters, including N stage ($P = 0.891$) or M stage ($P = 0.833$). These results demonstrate that the risk score is closely associated with the progression of HNSCC. Next, a nomogram containing the risk score and clinicopathological parameters was constructed (Figure 5H).

Table 2. The seven genes associated with the risk model in HNSCC.

ENSG ID	Symbol	Location	Expression status	Coefficient
ENSG00000142192	APP	Chromosome 21	Upregulated	0.0026
ENSG00000147889	CDKN2A	Chromosome 9	Upregulated	-0.0132
ENSG00000146648	EGFR	Chromosome 7	Upregulated	0.0016
ENSG00000144381	HSPD1	Chromosome 2	Upregulated	0.0048
ENSG00000147168	IL2RG	Chromosome X	Upregulated	-0.0113
ENSG00000122861	PLAU	Chromosome 10	Upregulated	0.0017
ENSG00000112715	VEGFA	Chromosome 6	Upregulated	0.0215

GSEA of risk score-related signaling pathways

GSEA was performed to identify significantly enriched pathways in the high-risk and low-risk groups in the TCGA data set. Thirty enriched pathways in the high-risk and low-risk groups were evaluated (Supplementary Table 5). Enriched pathways with significant differences (FDR < 0.25, NOM p < 0.05) were selected (Table 4). The results demonstrated that galactose metabolism, nitrogen metabolism, ERBB signaling pathway and pathways in cancer were significantly enriched in the high-risk group (Figure 6A, 6B) and that arachidonic acid metabolism, fatty acid metabolism, linoleic acid metabolism, B cell receptor signaling pathway, T cell receptor signaling pathway, intestinal immune network for IgA production and cytokine_cytokine receptor interaction were significantly enriched in the low-risk group (Figure 6C, 6D). Interestingly, the B cell receptor signaling pathway and T cell receptor signaling pathway were enriched in the low-risk group (Figure 6E, 6F), which indicated that a high risk score may be associated with immunosuppression. Other individual GSEA diagrams are shown in Supplementary Figure 3.

Association between the risk score and tumor immunity

To investigate the association between the risk score and immune/stromal score, we used the ESTIMATE algorithm to evaluate the immune/stromal score of the TCGA data set. The low-risk group had higher immune scores in tumor samples than the high-risk group (P < 0.0001, Figure 7A). In addition, Spearman's rank test revealed that there was a significant negative correlation between the risk score and immune score in HNSCC samples (R = -0.39, P < 0.0001, Figure 7B). However, there was no significant correlation between the risk score and stromal score in HNSCC samples (R = 0.031, P = 0.031, Figure 7C). The correlation between the risk score and ESTIMATE score in HNSCC samples was also tested (R = -0.21, P < 0.0001, Figure 7D).

We estimated the composition fraction of tumor-infiltrating immune cell types of patients in the TCGA data set utilizing the CIBERSORT algorithm to compare the relationship between the risk score and immune cells (Figure 7E). The results showed that HNSCC samples in the high-risk group contained a lower fraction of naïve B cells (P < 0.05), CD8 T cells (P < 0.001), CD4 memory activated T cells (P < 0.001) and follicular helper T cells (P < 0.001) compared to those in the low-risk group. However, CD4 memory resting T cells exhibited the opposite result (P < 0.001). These results are consistent with those of the GSEA in Figure 6E, 6F, which showed that a high risk score was associated with immunosuppression.

Correlation of the five immune cells with genes in the risk model

Based on the association between the risk model and the above five immune cell types (Figure 8A), we analyzed the correlation of the five immune cells with the 7 genes of the risk model. HNSCC samples with high PLAU expression contained a lower fraction of naïve B cells, CD8 T cells, CD4 memory activated T cells and follicular helper T cells compared to those with low expression, and CD4 memory resting T cells exhibited the opposite result (all P < 0.05, Figure 8B), which was consistent with the risk score. HNSCC samples with high APP expression compared to those with low expression showed that except for naïve B cells (P = 0.247), the results were consistent with the result of the risk score (all P < 0.01, Figure 8C). Similarly, the results of EGFR, except naïve B cells (P = 0.254) and CD4 memory activated T cells (P = 0.254), were consistent with the result of the risk score (all P < 0.01, Figure 8D). However, the results of IL2RG, as a protective factor, were not consistent with the results of the risk score (Figure 8E). Furthermore, the results of CDKN2A, HSPD1 and VEGFA showed that there was no significant difference in the five immune cells between the patients with high and low expression (all P > 0.05, Figure 8F–8H). Hence, the aging-related

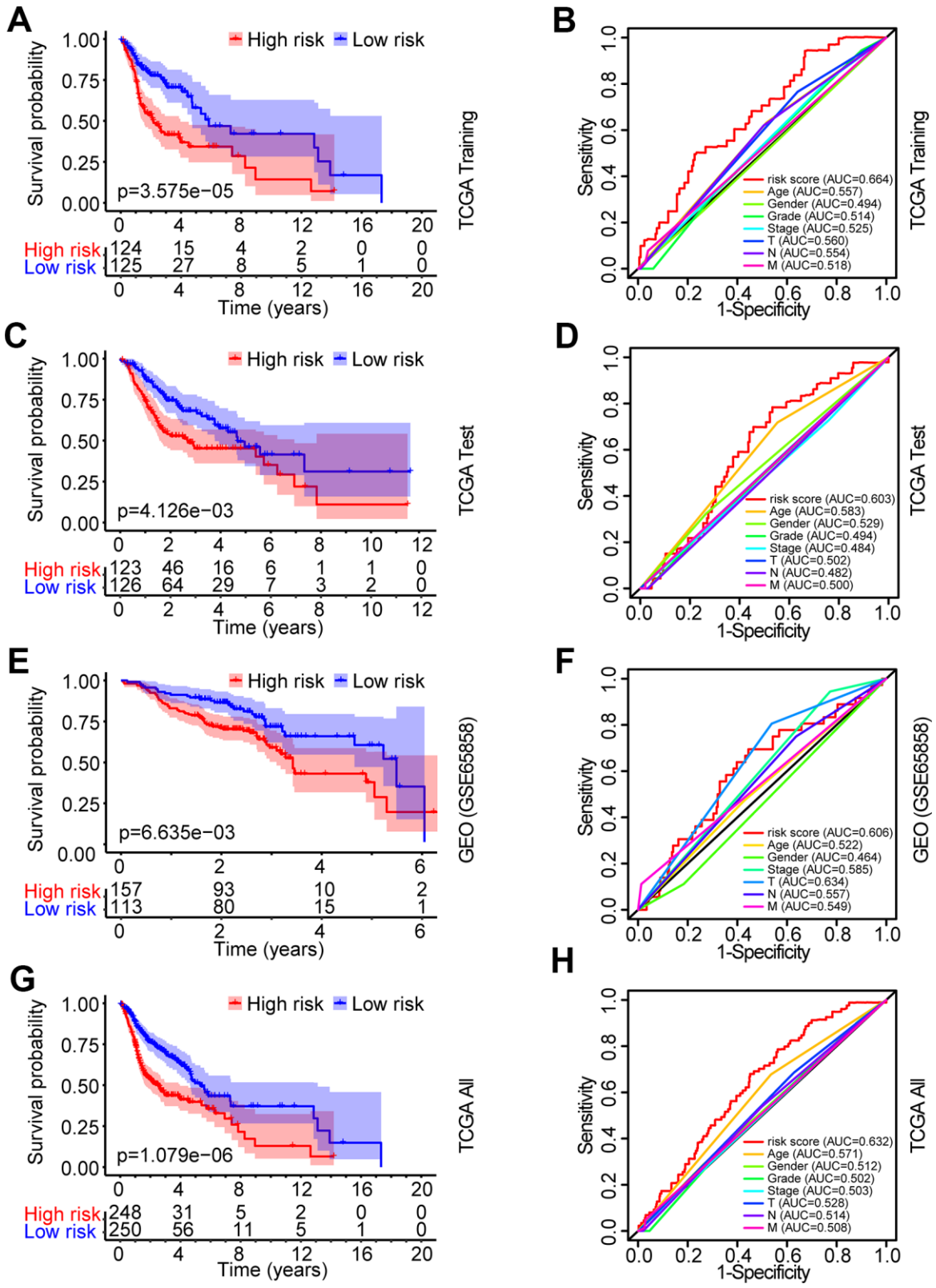

Figure 3. Identification and verification of the prognostic risk model in HNSCC. (**A**) Kaplan-Meier survival curve analysis of OS in the high-risk and low-risk groups of HNSCC patients in the TCGA training set. (**B**) ROC curve analysis and AUC for the risk score of AGs in the TCGA training set. (**C**, **E**, **G**) Kaplan-Meier survival curve analysis of OS in the high-risk and low-risk groups of HNSCC patients in the TCGA test set, GEO data set and TCGA all data set, respectively. (**D**, **F**, **H**) ROC curve analysis and AUC for the risk score of AGs in the TCGA test set, GEO data set and TCGA all data set, respectively.

genes PLAU, APP and EGFR play a key role in immunosuppression of HNSCC.

Correlation of proinflammatory factors with the risk score and genes of the risk model

Currently, accumulating studies have demonstrated that chronic inflammation related to cellular senescence plays a key role in tumor immunosuppression and major proinflammatory factors, including IL-1α, IL-1β, IL-6 and IL-8 [12–14]. Therefore, we investigated the correlation of major proinflammatory factors with the risk score and genes in the risk model. The results showed that mRNA expression levels of IL-1α, IL-1β, IL-6 and IL-8 in high-risk HNSCC samples were significantly higher than those in low-risk samples (all $P < 0.001$, Figure 9A). Consistent with the result of the risk score, the results of PLAU, APP and VEGFA also showed that the mRNA expression levels of IL-1α, IL-1β, IL-6 and IL-8 in HNSCC samples with high expression of PLAU, APP and VEGFA were significantly higher than those with low expression (all $P < 0.05$, Figure 9B–9D). Similarly, the results of EGFR, except for IL-6 ($P = 0.063$), were consistent

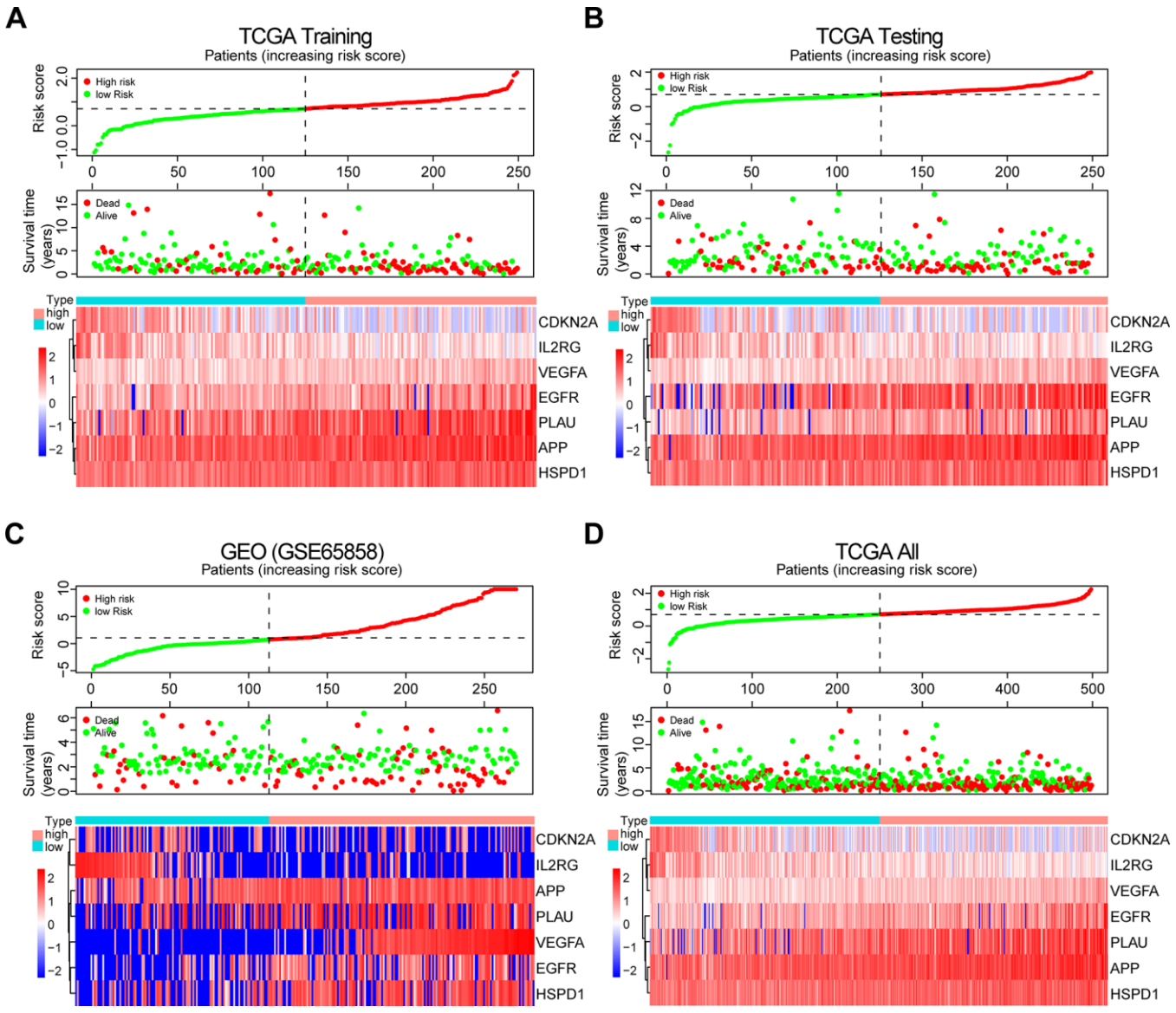

Figure 4. Prognosis and expression of risk genes in the high-risk and low-risk groups of HNSCC patients. (**A**) Risk plot distribution, survival status, and expression of risk genes of HNSCC patients in the TCGA training set. (**B**) Risk plot distribution, survival status, and expression of risk genes of HNSCC patients in the TCGA test set. (**C**) Risk plot distribution, survival status, and expression of risk genes of HNSCC patients in the GEO test set. (**D**) Risk plot distribution, survival status, and expression of risk genes of HNSCC patients in the TCGA all data set.

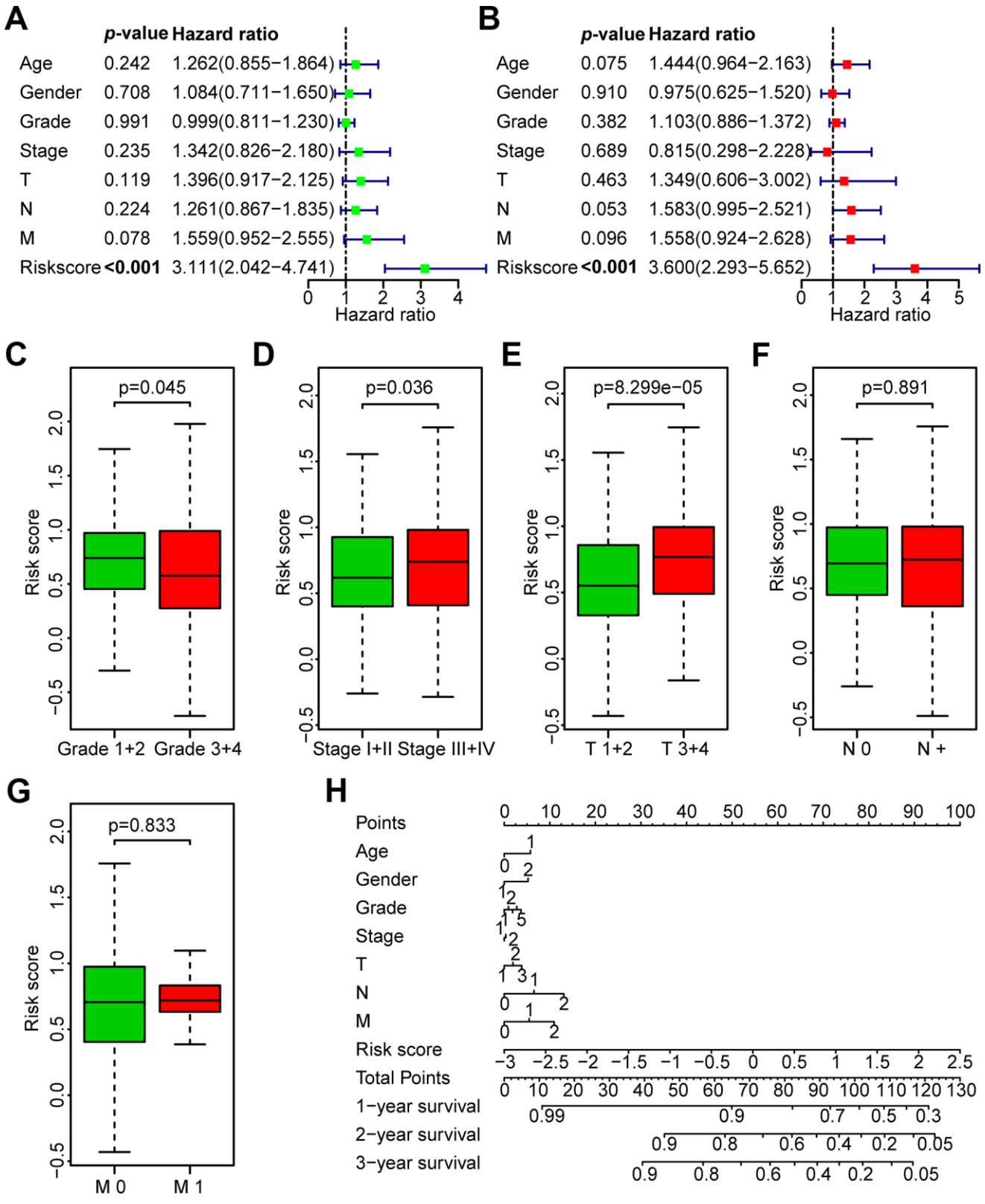

Figure 5. Correlation between the risk score and the clinicopathological characteristics of HNSCC patients. (**A**) Univariate Cox regression analysis of clinicopathological parameters of the patients in the TCGA training set. (**B**) Multivariate Cox regression analysis of the clinicopathological parameters of the patients in the TCGA training set. (**C**) Subgroup analysis of pathology grade (Grades 1+2 vs. Grades 3+4). (**D**) Subgroup analysis of clinical stage (Stages I+II vs. Stages III+IV). (**E**) Subgroup analysis of T classification (T 1+2 vs. T 3+4). (**F**) Subgroup analysis of N classification (N0 vs. N+). (**G**) Subgroup analysis of M classification (M 0 vs. M 1). (**H**) Nomogram for OS of HNSCC patients.

Table 3. Correlation between the clinicopathologic characteristics and the risk score (logistic regression) in HNSCC patients in the TCGA data set.

Clinical characteristics	Total (N)	Odds ratio in the risk score	*p*-value
Age (≥60 vs. <60)	498	1.016(0.713-1.448)	0.928
Gender	498	1.085 (0.729-1.619)	0.685
Grade (G1-2 vs. G3-4)	479	0.630 (0.413-0.953)	0.030
Stage (I-II vs. III-IV)	484	1.484 (0.972-2.278)	**0.039**
Local invasion (T1-2 vs. 3-4)	483	2.173 (1.490-3.188)	**0.000**
Lymph nodes (N0 vs. N+)	476	1.070 (0.747-1.533)	0.714
Distant metastasis (M0 vs. M1)	473	1.513 (0.248-11.564)	0.652

Table 4. Gene sets enriched in high and low risk scores.

MSigDB collection	Name	NES	ES	NOM *p*-value	FDR *q*-value
c2.cp.kegg.v7.1.symbols.gmt	KEGG_ERBB_SIGNALING_PATHWAY	1.658	0.460	0.024	0.197
	KEGG_PATHWAYS_IN_CANCER	1.619	0.406	0.022	0.193
	KEGG_GALACTOSE_METABOLISM	1.520	0.477	0.042	0.247
	KEGG_NITROGEN_METABOLISM	1.511	0.526	0.044	0.233
	KEGG_INTESTINAL_IMMUNE_NETWORK_FOR_IGA_PRODUCTION	-2.047	-0.761	0.000	0.016
	KEGG_ARACHIDONIC_ACID_METABOLISM	-1.916	-0.542	0.002	0.040
	KEGG_FATTY_ACID_METABOLISM	-1.668	-0.531	0.024	0.135
	KEGG_CYTOKINE_CYTOKINE_RECEPTOR_INTERACTION	-1.655	-0.446	0.033	0.139
	KEGG_T_CELL_RECEPTOR_SIGNALING_PATHWAY	-1.633	-0.494	0.042	0.126
	KEGG_B_CELL_RECEPTOR_SIGNALING_PATHWAY	-1.594	-0.491	0.048	0.128
	KEGG_LINOLEIC_ACID_METABOLISM	-1.593	-0.533	0.045	0.124

with the results of the risk score (all $P < 0.05$, Figure 9E). However, the results of IL2RG, HSPD1 and CDKN2A were either opposite of the results of the risk score, or there was no significant difference (Figure 9F–9H).

DISCUSSION

One key hallmark of cancer is the ability of cancer cells to evade immune destruction [26]. In the 1960s, studies showed that the aging process was associated with decreased immunological function [27–29]. Subsequently, accumulating studies have demonstrated that a chronic inflammatory microenvironment is involved in the aging process [30, 31]. Inflammation and asthenic immune surveillance with aging may facilitate tumor formation and development [9]. Currently, the role of the aging process in HNSCC is still ambiguous. Therefore, exploring the expression patterns of aging-related genes (AGs) is crucial for understanding the role of the aging process in HNSCC. Few studies have analyzed the correlation of AGs with HNSCC. Furthermore, the correlation of the expression of AGs with the prognosis of HNSCC patients has not been systematically investigated.

In this study, we initially performed a comprehensive investigation of the associations between 41 differentially expressed AGs (DEAGs, Figure 1A, 1B) and HNSCC prognosis and constructed a prognosis risk model with seven AGs, including APP, CDKN2A, EGFR, HSPD1, IL2RG, PLAU and VEGFA (Figure 1C) that revealed a robust performance signature for predicting prognosis

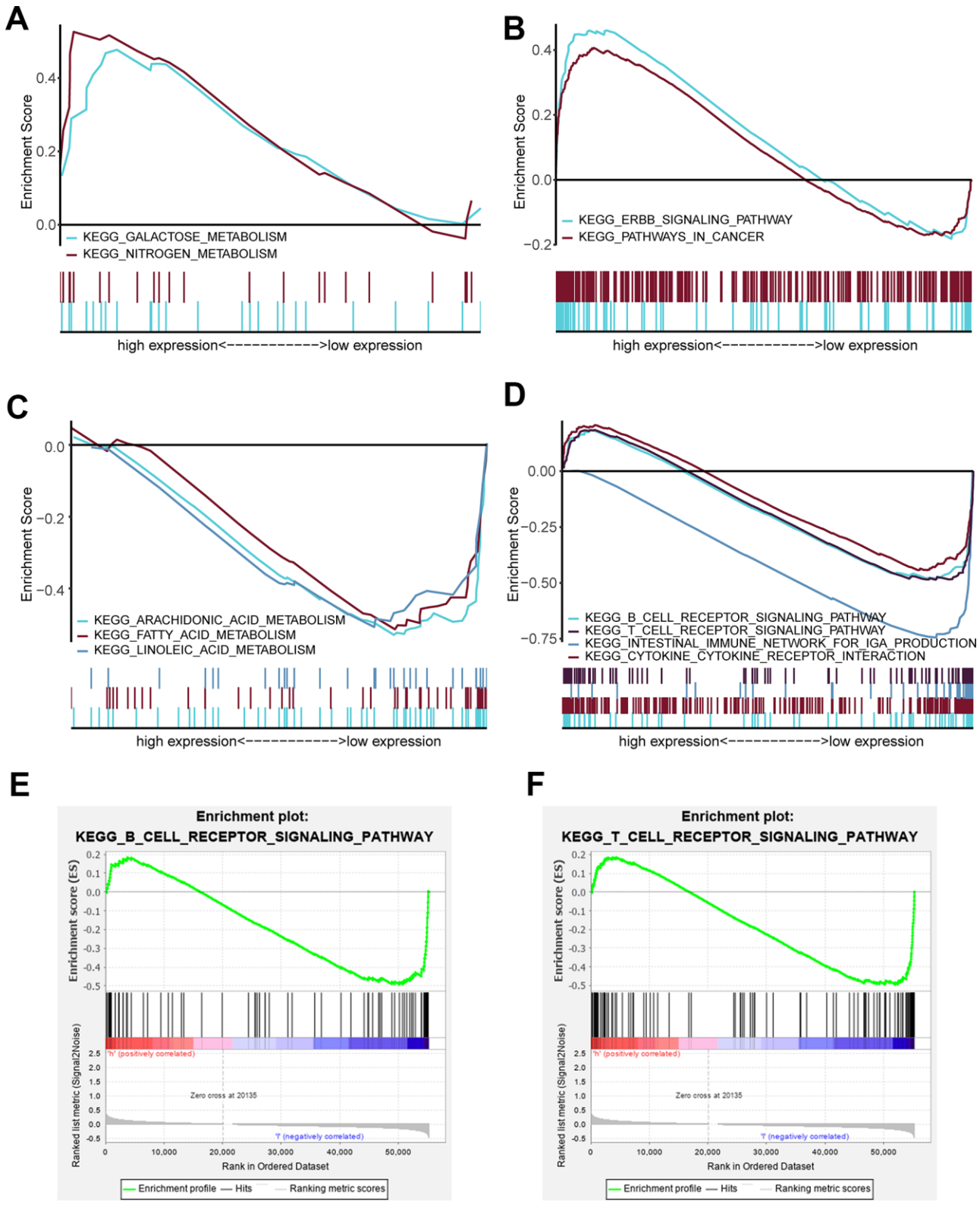

Figure 6. Enriched pathways of the high-risk and low-risk groups via GSEA. (**A**) Multiple GSEA for metabolism of the high-risk group: galactose metabolism and nitrogen metabolism. (**B**) Multiple GSEA for cancer pathways of the high-risk group: the ERBB signaling pathway and pathway in cancer. (**C**) Multiple GSEA for metabolism of the low-risk group: arachidonic acid metabolism, fatty acid metabolism and linoleic acid metabolism. (**D**) Multiple GSEA for inflammation and immunity of the low-risk group: the B cell receptor signaling pathway, T cell receptor signaling pathway, intestinal immune network for IgA production and cytokine_cytokine receptor interaction. (**E**) Single GSEA showing the B cell receptor signaling pathway. (**F**) Single GSEA showing the T cell receptor signaling pathway.

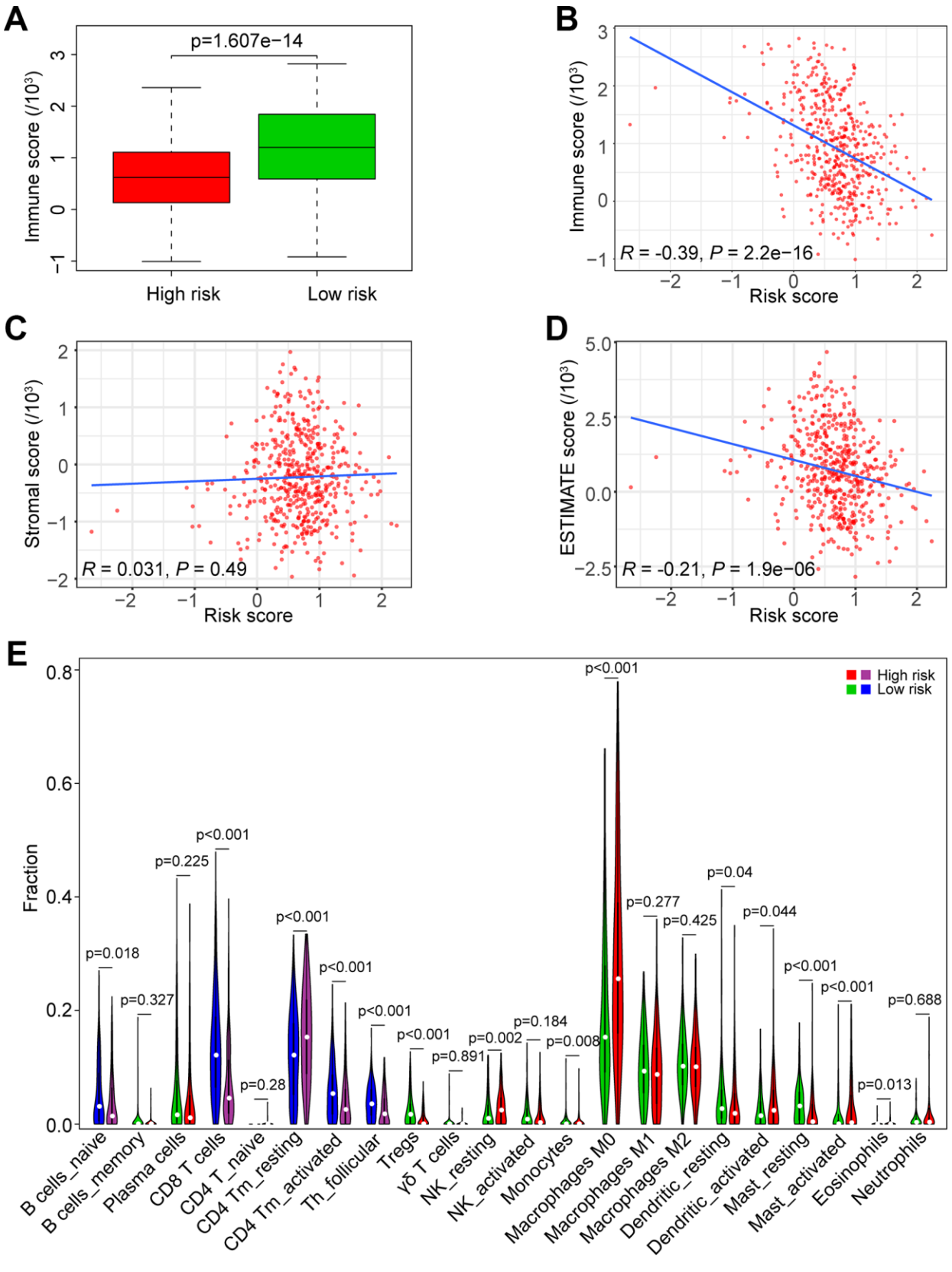

Figure 7. Association of the risk score with tumor immunity in the TCGA data set. (**A**) Distribution of immune scores according to the risk score of HNSCC patients. (**B**) Correlation of the risk score with the immune score in HNSCC samples. (**C**) Correlation of the risk score with the stromal score in HNSCC samples. (**D**) Correlation of the risk score with the ESTIMATE score in HNSCC samples. (**E**) Comparisons of immune cells between the high-risk and low-risk groups.

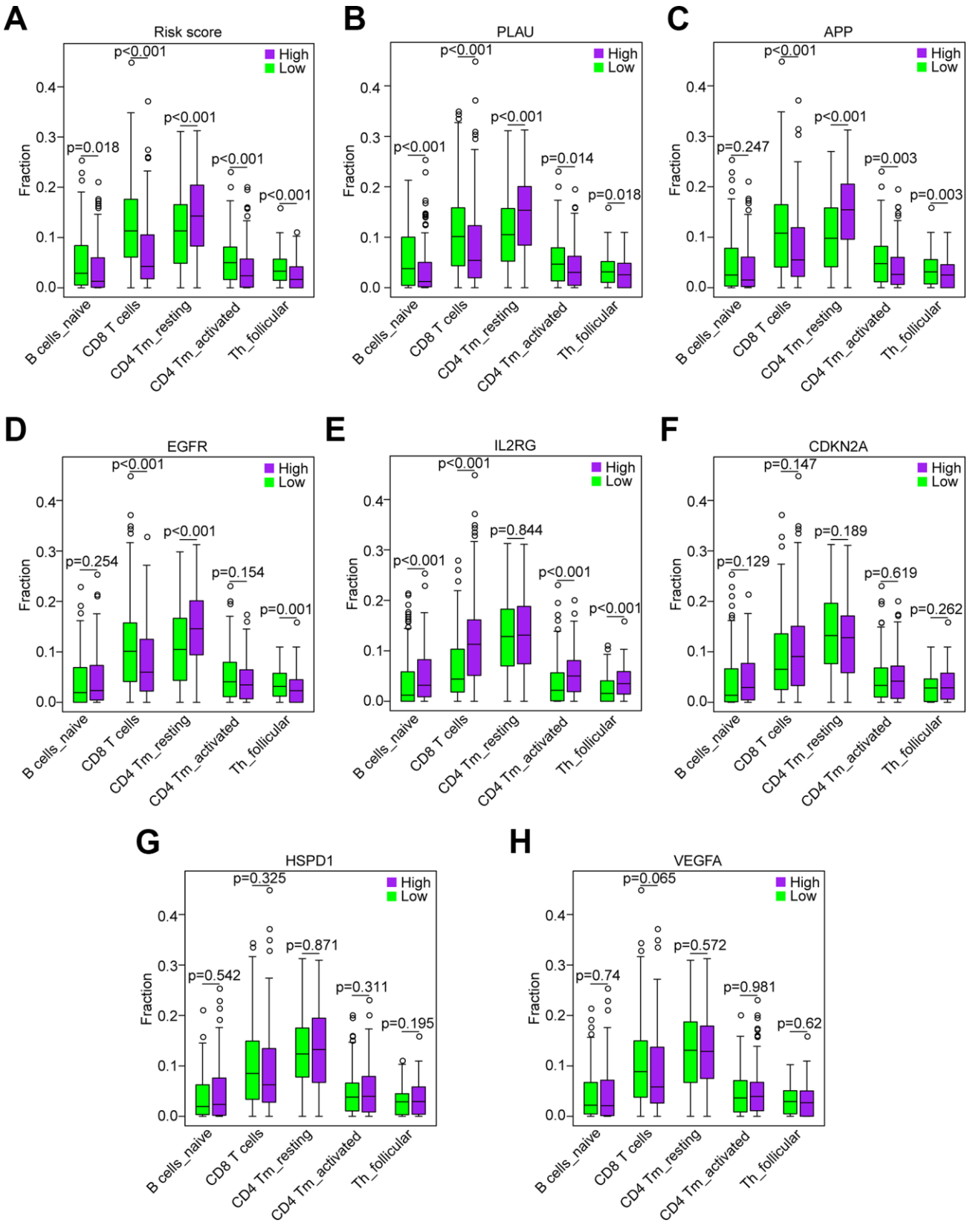

Figure 8. Correlation of the five immune cells with genes of the risk model in the TCGA data set. (**A**) Comparison of the five immune cells (naïve B cells, CD8 T cells, CD4 memory activated T cells and follicular helper T cells) between the high-risk and low-risk groups. (**B–H**) Distribution of the five immune cells based on the high expression and low expression of PLAU, APP, EGFR, IL2RG, CDKN2A, HSPD1 and VEGFA.

compared to clinicopathological factors in training and multiple validation sets (Figure 3).

In the prognostic risk model, CDKN2A and IL2RG acted as protective factors, while APP, PLAU, VEGFA, EGFR and HSPD1 were risk factors (Figure 4). CDKN2A, upregulated by Lupeol, had been shown to cause cell cycle arrest at G1 phase, mediating antitumor effects in HNSCC [32]. Low CDKN2A expression predicted poor survival independently of other clinical

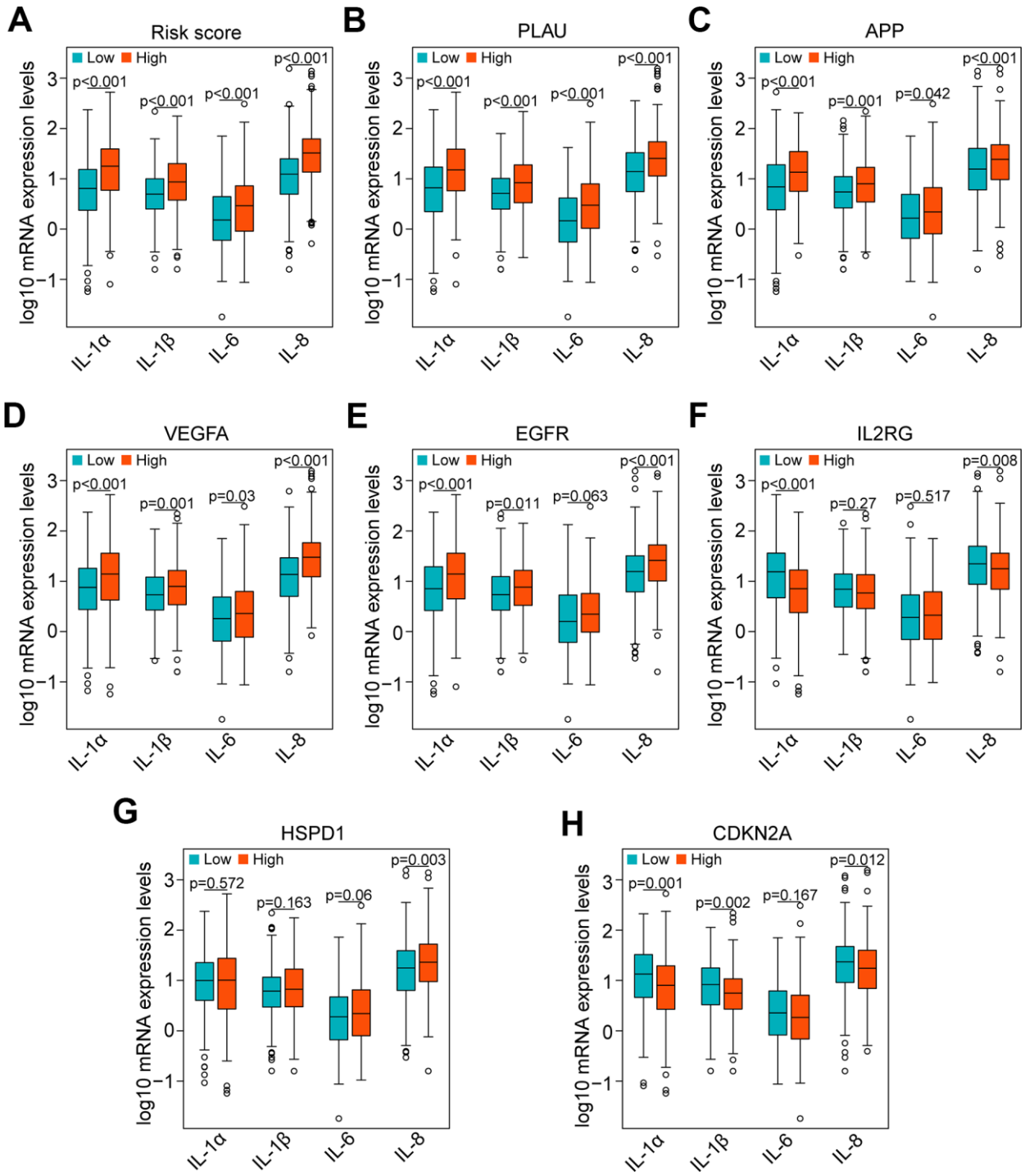

Figure 9. Correlation of proinflammatory factors with the risk score and genes of the risk model in the TCGA data set. (**A**) Comparison of the main proinflammatory factors (IL-1α, IL-1β, IL-6 and IL-8) between the high-risk and low-risk groups. (**B**–**H**) Distribution of the main proinflammatory factors based on high and low expression of PLAU, APP, VEGFA, EGFR, IL2RG, HSPD1 and CDKN2A.

factors in HPV-negative HNSCC [33]. IL2RG knockout mice showed immunodeficiency [34] and high tumorigenic engraftment efficiency of human cancer cells and tissues [35]. These studies are consistent with our results, suggesting that CDKN2A and IL2RG are anticancer genes. Previous studies showed that APP, a protein that originates β-amyloid that constitutes amyloid plaques, acts as one of the main pathological features of AD, one of the major aging-related diseases [36]. Interestingly, APP depletion causes cell cycle arrest in breast cancer cells and non-small cell lung cancer [37, 38]. PLAU has been identified as a biomarker of HNSCC [39], but its relationship to inflammation and immunity has not been explored. VEGFA was demonstrated to be involved in age-related macular degeneration (AMD), a leading cause of visual impairment in aging populations [40]. Indeed, VEGFA is a key molecule in various signaling pathways promoting the progression of multiple cancers [41–43]. EGFR is a biomarker in HNSCC [44] and enhances the progression of HNSCC by mediating a variety of signaling pathways [45–47]. HSPD1 was closely related to prognosis in both oral squamous cell carcinoma and breast cancer [48, 49]. Our study was the first to suggest that these factors represent a prognostic risk model of HNSCC.

Interestingly, our GSEA results revealed that B cell receptor (BCR) signaling and T cell receptor (TCR) signaling pathways were enriched in the low-risk group (Figure 6E, 6F), indicating that they may be inhibited in the high-risk group. BCR and TCR signaling is crucial for B cell and T cell proliferation and for development of adaptive immunity, and their abnormalities could lead to immunodeficiency [50–53]. For these reasons, we investigated correlation of the risk score with the immune score and the composition fraction of tumor-infiltrating immune cell types in HNSCC samples of TCGA data set. As we confirm here, there was a negative correlation between the risk score, and the immune and high-risk group contained lower fractions of naïve B cells, CD8 T cells, CD4 memory activated T cells and follicular helper T and a higher fraction of CD4 memory resting T cells compared to the low-risk group (Figure 7). Hence, our study revealed a significant correlation between a high risk score and immunosuppression and its association with the growth and differentiation of B and T cells, and high expression of PLAU, APP and EGFR were the main factors of tumor immunosuppression (Figure 8). Previous work unveiled that PLAU is particularly important for memory regulatory T cells (Tregs) [54]; however, there was no investigation of other immune cells. Based on an Alzheimer's transgenic mouse, PLAU was demonstrated as an impact factor of adaptive immunity, involved in lacking functional B and T cells [55]. The EGFR monoclonal antibody, Cetuximab, triggered immunogenic cell death [56], suggesting that EGFR plays an important role in immune cells survival. The proinflammatory factors of the senescence associated secretory phenotype (SASP) facilitate tumor immunosuppression [30, 31]. We confirmed that a high risk score was significantly associated with mRNA expression levels of IL-1α, IL-1β, IL-6 and IL-8 in HNSCC samples, and the results of PLAU, APP, VEGFA and EGFR were consistent with the results of the risk score (Figure 9).

Although we identified a prognostic risk model with seven AGs and confirmed that the risk model was significantly associated with inflammation and immunosuppression, this work has limitations. The study conducted with bioinformatics analysis was not robust enough and needs to be confirmed via experimental verification. Hence, further laboratory experiments, including a multicenter study with larger sample sizes, are needed.

In summary, in this study, we developed a robust prognostic risk model with 7 AGs. Compared to other clinical parameters, the risk score is an independent prognostic index. Furthermore, a high risk score indicates the chronic inflammatory and immunosuppressive state of HNSCC patients. Therefore, this risk model may serve as a prognostic signature and provide clues for individualized immunotherapy for HNSCC patients.

CONCLUSIONS

In conclusion, in our study, we developed a prognostic risk model with 7 differentially expressed AGs, which has great potential as an immunosuppressive and inflammatory state biomarker in HNSCC patients and provides insight into individualized immunotherapy for HNSCC patients.

MATERIALS AND METHODS

Data sets

We obtained 307 human AGs from the human aging genome resource (HAGR, http://genomics.senescence.info/genes/, Supplementary Table 1). The RNA sequencing (RNA-Seq) expression profile data set was downloaded from the TCGA database (https://portal.gdc.cancer.gov/) of 500 HNSCC patients (2 duplicate patients were removed) with 44 paracarcinoma samples, and clinical information was downloaded from the cBioPortal database (https://www.cbioportal.org/). For TCGA data, 498 HNSCC patients with follow-up data were selected and randomly divided

into two groups: the TCGA training set (n=298, Supplementary Table 3) and the TCGA test set (n=298, Supplementary Table 4). The GSE65858 data set as an independent verification set was obtained from the Gene Expression Omnibus (GEO) database (https://www.ncbi.nlm.nih.gov/geo/) and included RNA-Seq data and clinical information. We performed data analysis utilizing R software (version 3.6.3, https://www.r-project.org/).

Differentially expressed gene (DEG) analysis

We evaluated differentially expressed aging-related genes (DEAGs) between HNSCC and normal samples using the Wilcoxon test in the limma package. Cut-off values were adjusted with the false discovery rate (FDR) [19]. FDR < 0.05, and |log FC| value > 1 was defined as significant. Then, we constructed a hierarchical cluster heat map via the "pheatmap" package and a volcano plot to visualize the results of the DEAGs. The distribution of the DEAGs on chromosomes was visualized via the "OmicCircos" R package [20].

GO and KEGG pathway analyses

Gene Ontology (GO) and Kyoto Encyclopedia of Genes and Genomes (KEGG) pathway enrichment analyses were implemented with the "enrichplot" R package [21] to analyze the function of the DEAGs. GO terms contained biological process (BP), cellular component (CC) and molecular function (MF). For the analysis results, both *P*-value and false discovery rate (FDR) values < 0.05 were defined as statistically significant.

Construction of a prognostic gene signature

To identify survival-associated DEAGs, we conducted univariate Cox regression analysis. Candidate prognostic genes were selected with a threshold value of $P < 0.05$. Then, Lasso regression analysis in the TCGA training set was executed, and a multigene prognostic signature was constructed. The individualized risk score was calculated with the regression coefficients of each gene using the following computational formula:

$$Risk\ score = \sum_{k=1}^{n} coefficient\ (gene_k) * Exp_k$$

where n is the number of the candidate prognostic genes, $gene_k$ is the $_k$th candidate genes, coefficient is the estimated regression coefficient of genes from the multivariate Cox regression analysis, and Exp_k is the expression value of the $_k$th candidate genes. Based on the median the risk score of the TCGA training set, the HNSCC patients were divided into high-risk and low-risk groups. The association between the candidate genes and risk scores were shown by a hierarchical cluster heat map, and a nomogram containing the risk score of prognostic AGs and clinicopathological parameters was constructed via the "rms" R package.

Gene Set Enrichment Analysis

GSEA is a powerful analytical method used for estimating significant differences between two biological conditions to determine specific functional gene sets [22]. In the current study, GSEA was performed using GSEA software (v4.0.3) (https://www.gsea-msigdb.org/gsea/downloads.jsp) with the Molecular Signatures Database (MSigDB) [23] C2 curated gene sets, which generated a list of significantly different gene sets between the high-risk and low-risk groups. Each gene set was permutated 1000 times for each analysis. Gene sets with *p*-value < 0.05 and FDR < 0.25 were considered significantly enriched.

Evaluation of immune scores and immune cell infiltration

The ESTIMATE (Estimation of Stromal and Immune cells in Malignant Tumor tissues using Expression data) algorithm is a tool developed to evaluate immune and stromal scores in tumor samples. We calculated the immune and stromal ESTIMATE scores based on TCGA gene expression data using the "estimate" R package [24].

CIBERSORT is an analytical method used for characterizing the cellular composition of complex tissues based on gene expression profiles [25]. We conducted an estimation of the composition fraction of tumor- infiltrating immune cell types of each patient using the CIBERSORT algorithm (http://cibersort.stanford.edu/).

Statistical analysis

All statistical analyses were performed using R-3.6.3. The distribution differences among the variables were analyzed by chi-square test or Fisher's exact test. The Kaplan-Meier curve with the log-rank test was used to estimate survival analysis. Univariate and multivariate Cox regression analyses were performed to analyze the relationship between given factors and survival in HNSCC patients. ROC curve analysis was used to evaluate the diagnostic value of the risk model. Spearman's rank correlation test was estimated to assess the correlation between variables. $P < 0.05$ was identified as statistically significant.

Data Availability Statement

Expression profile datasets for this study can be accessed from The Cancer Genome Atlas (TCGA) (https://portal.gdc.cancer.gov/) and Gene Expression Omnibus (GEO) database (https://www.ncbi.nlm.nih.gov/geo/), and aging-related genes (AGs) can be retrieved from the Human Aging Genome Resources (HAGR, http://genomics.senescence.info/genes/).

AUTHOR CONTRIBUTIONS

Zhifeng Liu and Runliang Gan contributed to project design and final approval of the manuscript. Jing Yang, Qingshan Jiang, Lijun Liu, Hong Peng, Yaya Wang, Shuyan Li, Yanhua Tang and Jing Yu performed data analysis, interpretation, visualization and drafting.

CONFLICTS OF INTEREST

All authors declare that they have no conflicts of interest.

FUNDING

This work was supported by grants from the Health and Family Planning Commission of Hunan Province (20201921, 20201947, B20180186), the Natural Science Foundation of Hunan Province (2019JJ50547), the Hunan Province Key Laboratory of Tumor Cellular and Molecular Pathology (2016TP1015), the Hunan Provincial Science and Technology Department (2017Sk50206) and the National Natural Science Foundation of China (81372134).

REFERENCES

1. Bray F, Ferlay J, Soerjomataram I, Siegel RL, Torre LA, Jemal A. Global cancer statistics 2018: GLOBOCAN estimates of incidence and mortality worldwide for 36 cancers in 185 countries. CA Cancer J Clin. 2018; 68:394–424. https://doi.org/10.3322/caac.21492 PMID:30207593

2. Cramer JD, Burtness B, Le QT, Ferris RL. The changing therapeutic landscape of head and neck cancer. Nat Rev Clin Oncol. 2019; 16:669–83. https://doi.org/10.1038/s41571-019-0227-z PMID:31189965

3. Hill SJ, D'Andrea AD. Predictive potential of head and neck squamous cell carcinoma organoids. Cancer Discov. 2019; 9:828–30. https://doi.org/10.1158/2159-8290.CD-19-0527 PMID:31262743

4. Siegel RL, Miller KD, Jemal A. Cancer statistics, 2020. CA Cancer J Clin. 2020; 70:7–30. https://doi.org/10.3322/caac.21590 PMID:31912902

5. López-Otín C, Blasco MA, Partridge L, Serrano M, Kroemer G. The hallmarks of aging. Cell. 2013; 153:1194–217. https://doi.org/10.1016/j.cell.2013.05.039 PMID:23746838

6. Lee S, Schmitt CA. The dynamic nature of senescence in cancer. Nat Cell Biol. 2019; 21:94–101. https://doi.org/10.1038/s41556-018-0249-2 PMID:30602768

7. Baker DJ, Childs BG, Durik M, Wijers ME, Sieben CJ, Zhong J, Saltness RA, Jeganathan KB, Verzosa GC, Pezeshki A, Khazaie K, Miller JD, van Deursen JM. Naturally occurring p16(Ink4a)-positive cells shorten healthy lifespan. Nature. 2016; 530:184–89. https://doi.org/10.1038/nature16932 PMID:26840489

8. Serrano M, Lin AW, McCurrach ME, Beach D, Lowe SW. Oncogenic ras provokes premature cell senescence associated with accumulation of p53 and p16INK4a. Cell. 1997; 88:593–602. https://doi.org/10.1016/s0092-8674(00)81902-9 PMID:9054499

9. Kuilman T, Michaloglou C, Vredeveld LC, Douma S, van Doorn R, Desmet CJ, Aarden LA, Mooi WJ, Peeper DS. Oncogene-induced senescence relayed by an interleukin-dependent inflammatory network. Cell. 2008; 133:1019–31. https://doi.org/10.1016/j.cell.2008.03.039 PMID:18555778

10. Coppé JP, Patil CK, Rodier F, Sun Y, Muñoz DP, Goldstein J, Nelson PS, Desprez PY, Campisi J. Senescence-associated secretory phenotypes reveal cell-nonautonomous functions of oncogenic RAS and the p53 tumor suppressor. PLoS Biol. 2008; 6:2853–68. https://doi.org/10.1371/journal.pbio.0060301 PMID:19053174

11. Laberge RM, Zhou L, Sarantos MR, Rodier F, Freund A, de Keizer PL, Liu S, Demaria M, Cong YS, Kapahi P, Desprez PY, Hughes RE, Campisi J. Glucocorticoids suppress selected components of the senescence-associated secretory phenotype. Aging Cell. 2012; 11:569–78. https://doi.org/10.1111/j.1474-9726.2012.00818.x PMID:22404905

12. Mahmoudi S, Xu L, Brunet A. Turning back time with emerging rejuvenation strategies. Nat Cell Biol. 2019; 21:32–43. https://doi.org/10.1038/s41556-018-0206-0 PMID:30602763

13. Ovadya Y, Landsberger T, Leins H, Vadai E, Gal H, Biran A, Yosef R, Sagiv A, Agrawal A, Shapira A, Windheim J,

Tsoory M, Schirmbeck R, et al. Impaired immune surveillance accelerates accumulation of senescent cells and aging. Nat Commun. 2018; 9:5435. https://doi.org/10.1038/s41467-018-07825-3 PMID:30575733

14. Faget DV, Ren Q, Stewart SA. Unmasking senescence: context-dependent effects of SASP in cancer. Nat Rev Cancer. 2019; 19:439–53. https://doi.org/10.1038/s41568-019-0156-2 PMID:31235879

15. Ko LJ, Prives C. P53: puzzle and paradigm. Genes Dev. 1996; 10:1054–72. https://doi.org/10.1101/gad.10.9.1054 PMID:8654922

16. Henriksson M, Lüscher B. Proteins of the Myc network: essential regulators of cell growth and differentiation. Adv Cancer Res. 1996; 68:109–82. https://doi.org/10.1016/s0065-230x(08)60353-x PMID:8712067

17. Johnson SC, Rabinovitch PS, Kaeberlein M. mTOR is a key modulator of ageing and age-related disease. Nature. 2013; 493:338–45. https://doi.org/10.1038/nature11861 PMID:23325216

18. Tacutu R, Thornton D, Johnson E, Budovsky A, Barardo D, Craig T, Diana E, Lehmann G, Toren D, Wang J, Fraifeld VE, de Magalhães JP. Human ageing genomic resources: new and updated databases. Nucleic Acids Res. 2018; 46:D1083–90. https://doi.org/10.1093/nar/gkx1042 PMID:29121237

19. Nakamura A, Osonoi T, Terauchi Y. Relationship between urinary sodium excretion and pioglitazone-induced edema. J Diabetes Investig. 2010; 1:208–11. https://doi.org/10.1111/j.2040-1124.2010.00046.x PMID:24843434

20. Hu Y, Yan C, Hsu CH, Chen QR, Niu K, Komatsoulis GA, Meerzaman D. OmicCircos: a simple-to-use R package for the circular visualization of multidimensional omics data. Cancer Inform. 2014; 13:13–20. https://doi.org/10.4137/CIN.S13495 PMID:24526832

21. Yu G, Wang LG, Han Y, He QY. clusterProfiler: an R package for comparing biological themes among gene clusters. OMICS. 2012; 16:284–87. https://doi.org/10.1089/omi.2011.0118 PMID:22455463

22. Subramanian A, Tamayo P, Mootha VK, Mukherjee S, Ebert BL, Gillette MA, Paulovich A, Pomeroy SL, Golub TR, Lander ES, Mesirov JP. Gene set enrichment analysis: a knowledge-based approach for interpreting genome-wide expression profiles. Proc Natl Acad Sci USA. 2005; 102:15545–50. https://doi.org/10.1073/pnas.0506580102 PMID:16199517

23. Liberzon A, Subramanian A, Pinchback R, Thorvaldsdóttir H, Tamayo P, Mesirov JP. Molecular signatures database (MSigDB) 3.0. Bioinformatics. 2011; 27:1739–40. https://doi.org/10.1093/bioinformatics/btr260 PMID:21546393

24. Yoshihara K, Shahmoradgoli M, Martínez E, Vegesna R, Kim H, Torres-Garcia W, Treviño V, Shen H, Laird PW, Levine DA, Carter SL, Getz G, Stemke-Hale K, et al. Inferring tumour purity and stromal and immune cell admixture from expression data. Nat Commun. 2013; 4:2612. https://doi.org/10.1038/ncomms3612 PMID:24113773

25. Newman AM, Liu CL, Green MR, Gentles AJ, Feng W, Xu Y, Hoang CD, Diehn M, Alizadeh AA. Robust enumeration of cell subsets from tissue expression profiles. Nat Methods. 2015; 12:453–57. https://doi.org/10.1038/nmeth.3337 PMID:25822800

26. Hanahan D, Weinberg RA. Hallmarks of cancer: the next generation. Cell. 2011; 144:646–74. https://doi.org/10.1016/j.cell.2011.02.013 PMID:21376230

27. Mackay IR. Ageing and immunological function in man. Gerontologia. 1972; 18:285–304. https://doi.org/10.1159/000211941 PMID:4549306

28. Inkeles B, Innes JB, Kuntz MM, Kadish AS, Weksler ME. Immunological studies of aging. Iii. Cytokinetic basis for the impaired response of lymphocytes from aged humans to plant lectins. J Exp Med. 1977; 145:1176–87. https://doi.org/10.1084/jem.145.5.1176 PMID:300780

29. Roder JC, Duwe AK, Bell DA, Singhal SK. Immunological senescence. I. The role of suppressor cells. Immunology. 1978; 35:837–47. PMID:363607

30. Franceschi C, Bonafè M, Valensin S, Olivieri F, De Luca M, Ottaviani E, De Benedictis G. Inflamm-aging. An evolutionary perspective on immunosenescence. Ann N Y Acad Sci. 2000; 908:244–54. https://doi.org/10.1111/j.1749-6632.2000.tb06651.x PMID:10911963

31. Franceschi C, Garagnani P, Parini P, Giuliani C, Santoro A. Inflammaging: a new immune-metabolic viewpoint for age-related diseases. Nat Rev Endocrinol. 2018; 14:576–90. https://doi.org/10.1038/s41574-018-0059-4 PMID:30046148

32. Bhattacharyya S, Sekar V, Majumder B, Mehrotra DG, Banerjee S, Bhowmick AK, Alam N, Mandal GK, Biswas J, Majumder PK, Murmu N. CDKN2A-p53 mediated antitumor effect of lupeol in head and neck cancer. Cell Oncol (Dordr). 2017; 40:145–55.

https://doi.org/10.1007/s13402-016-0311-7 PMID:28039610

33. Chen WS, Bindra RS, Mo A, Hayman T, Husain Z, Contessa JN, Gaffney SG, Townsend JP, Yu JB. CDKN2A copy number loss is an independent prognostic factor in HPV-negative head and neck squamous cell carcinoma. Front Oncol. 2018; 8:95. https://doi.org/10.3389/fonc.2018.00095 PMID:29670856

34. Byambaa S, Uosaki H, Hara H, Nagao Y, Abe T, Shibata H, Nureki O, Ohmori T, Hanazono Y. Generation of novel Il2rg-knockout mice with clustered regularly interspaced short palindromic repeats (CRISPR) and Cas9. Exp Anim. 2020; 69:189–98. https://doi.org/10.1538/expanim.19-0120 PMID:31801915

35. Zhou Q, Facciponte J, Jin M, Shen Q, Lin Q. Humanized NOD-SCID IL2rg–/– mice as a preclinical model for cancer research and its potential use for individualized cancer therapies. Cancer Lett. 2014; 344:13–19. https://doi.org/10.1016/j.canlet.2013.10.015 PMID:24513265

36. Galvão F Jr, Grokoski KC, da Silva BB, Lamers ML, Siqueira IR. The amyloid precursor protein (APP) processing as a biological link between Alzheimer's disease and cancer. Ageing Res Rev. 2019; 49:83–91. https://doi.org/10.1016/j.arr.2018.11.007 PMID:30500566

37. Lim S, Yoo BK, Kim HS, Gilmore HL, Lee Y, Lee HP, Kim SJ, Letterio J, Lee HG. Amyloid-β precursor protein promotes cell proliferation and motility of advanced breast cancer. BMC Cancer. 2014; 14:928. https://doi.org/10.1186/1471-2407-14-928 PMID:25491510

38. Sobol A, Galluzzo P, Weber MJ, Alani S, Bocchetta M. Depletion of amyloid precursor protein (APP) causes G0 arrest in non-small cell lung cancer (NSCLC) cells. J Cell Physiol. 2015; 230:1332–41. https://doi.org/10.1002/jcp.24875 PMID:25502341

39. Yang K, Zhang S, Zhang D, Tao Q, Zhang T, Liu G, Liu X, Zhao T. Identification of SERPINE1, PLAU and ACTA1 as biomarkers of head and neck squamous cell carcinoma based on integrated bioinformatics analysis. Int J Clin Oncol. 2019; 24:1030–41. https://doi.org/10.1007/s10147-019-01435-9 PMID:30937621

40. Zhao L, Grob S, Avery R, Kimura A, Pieramici D, Lee J, Rabena M, Ortiz S, Quach J, Cao G, Luo H, Zhang M, Pei M, et al. Common variant in VEGFA and response to anti-VEGF therapy for neovascular age-related macular degeneration. Curr Mol Med. 2013; 13:929–34. https://doi.org/10.2174/15665240113139990048 PMID:23745581

41. Wang LL, Zong ZH, Liu Y, Guan X, Chen S, Zhao Y. CircRhoC promotes tumorigenicity and progression in ovarian cancer by functioning as a miR-302e sponge to positively regulate VEGFA. J Cell Mol Med. 2019; 23:8472–81. https://doi.org/10.1111/jcmm.14736 PMID:31639291

42. Zhang Q, Lu S, Li T, Yu L, Zhang Y, Zeng H, Qian X, Bi J, Lin Y. ACE2 inhibits breast cancer angiogenesis via suppressing the VEGFa/VEGFR2/ERK pathway. J Exp Clin Cancer Res. 2019; 38:173. https://doi.org/10.1186/s13046-019-1156-5 PMID:31023337

43. Wu H, Wei M, Jiang X, Tan J, Xu W, Fan X, Zhang R, Ding C, Zhao F, Shao X, Zhang Z, Shi R, Zhang W, Wu G. lncRNA PVT1 promotes tumorigenesis of colorectal cancer by stabilizing miR-16-5p and interacting with the VEGFA/VEGFR1/AKT axis. Mol Ther Nucleic Acids. 2020; 20:438–50. https://doi.org/10.1016/j.omtn.2020.03.006 PMID:32276209

44. Beck TN, Georgopoulos R, Shagisultanova EI, Sarcu D, Handorf EA, Dubyk C, Lango MN, Ridge JA, Astsaturov I, Serebriiskii IG, Burtness BA, Mehra R, Golemis EA. EGFR and RB1 as dual biomarkers in HPV-negative head and neck cancer. Mol Cancer Ther. 2016; 15:2486–97. https://doi.org/10.1158/1535-7163.MCT-16-0243 PMID:27507850

45. Barzegar M, Ma S, Zhang C, Chen X, Gu Y, Shang C, Jiang X, Yang J, Nathan CA, Yang S, Huang S. SKLB188 inhibits the growth of head and neck squamous cell carcinoma by suppressing EGFR signalling. Br J Cancer. 2017; 117:1154–63. https://doi.org/10.1038/bjc.2017.298 PMID:28873083

46. Nottingham LK, Yan CH, Yang X, Si H, Coupar J, Bian Y, Cheng TF, Allen C, Arun P, Gius D, Dang L, Van Waes C, Chen Z. Aberrant IKKα and IKKβ cooperatively activate NF-κB and induce EGFR/AP1 signaling to promote survival and migration of head and neck cancer. Oncogene. 2014; 33:1135–47. https://doi.org/10.1038/onc.2013.49 PMID:23455325

47. Wang D, Su L, Huang D, Zhang H, Shin DM, Chen ZG. Downregulation of E-cadherin enhances proliferation of head and neck cancer through transcriptional regulation of EGFR. Mol Cancer. 2011; 10:116. https://doi.org/10.1186/1476-4598-10-116 PMID:21939503

48. Kang BH, Shu CW, Chao JK, Lee CH, Fu TY, Liou HH, Ger LP, Liu PF. HSPD1 repressed E-cadherin expression to

promote cell invasion and migration for poor prognosis in oral squamous cell carcinoma. Sci Rep. 2019; 9:8932. https://doi.org/10.1038/s41598-019-45489-1 PMID:31222140

49. Kim SK, Kim K, Ryu JW, Ryu TY, Lim JH, Oh JH, Min JK, Jung CR, Hamamoto R, Son MY, Kim DS, Cho HS. The novel prognostic marker, EHMT2, is involved in cell proliferation via HSPD1 regulation in breast cancer. Int J Oncol. 2019; 54:65–76. https://doi.org/10.3892/ijo.2018.4608 PMID:30365075

50. Takeuchi Y, Hirota K, Sakaguchi S. Impaired T cell receptor signaling and development of T cell-mediated autoimmune arthritis. Immunol Rev. 2020; 294:164–76. https://doi.org/10.1111/imr.12841 PMID:31944330

51. Burger JA, Wiestner A. Targeting B cell receptor signalling in cancer: preclinical and clinical advances. Nat Rev Cancer. 2018; 18:148–67. https://doi.org/10.1038/nrc.2017.121 PMID:29348577

52. Berry CT, Liu X, Myles A, Nandi S, Chen YH, Hershberg U, Brodsky IE, Cancro MP, Lengner CJ, May MJ, Freedman BD. BCR-induced Ca^{2+} signals dynamically tune survival, metabolic reprogramming, and proliferation of naive B cells. Cell Rep. 2020; 31:107474. https://doi.org/10.1016/j.celrep.2020.03.038 PMID:32294437

53. Zikherman J, Parameswaran R, Weiss A. Endogenous antigen tunes the responsiveness of naive B cells but not T cells. Nature. 2012; 489:160–64. https://doi.org/10.1038/nature11311 PMID:22902503

54. He F, Chen H, Probst-Kepper M, Geffers R, Eifes S, Del Sol A, Schughart K, Zeng AP, Balling R. PLAU inferred from a correlation network is critical for suppressor function of regulatory T cells. Mol Syst Biol. 2012; 8:624. https://doi.org/10.1038/msb.2012.56 PMID:23169000

55. Späni C, Suter T, Derungs R, Ferretti MT, Welt T, Wirth F, Gericke C, Nitsch RM, Kulic L. Reduced β-amyloid pathology in an APP transgenic mouse model of Alzheimer's disease lacking functional B and T cells. Acta Neuropathol Commun. 2015; 3:71. https://doi.org/10.1186/s40478-015-0251-x PMID:26558367

56. Pozzi C, Cuomo A, Spadoni I, Magni E, Silvola A, Conte A, Sigismund S, Ravenda PS, Bonaldi T, Zampino MG, Cancelliere C, Di Fiore PP, Bardelli A, et al. The EGFR-specific antibody cetuximab combined with chemotherapy triggers immunogenic cell death. Nat Med. 2016; 22:624–31. https://doi.org/10.1038/nm.4078 PMID:27135741

SUPPLEMENTARY MATERIALS

Supplementary Figures

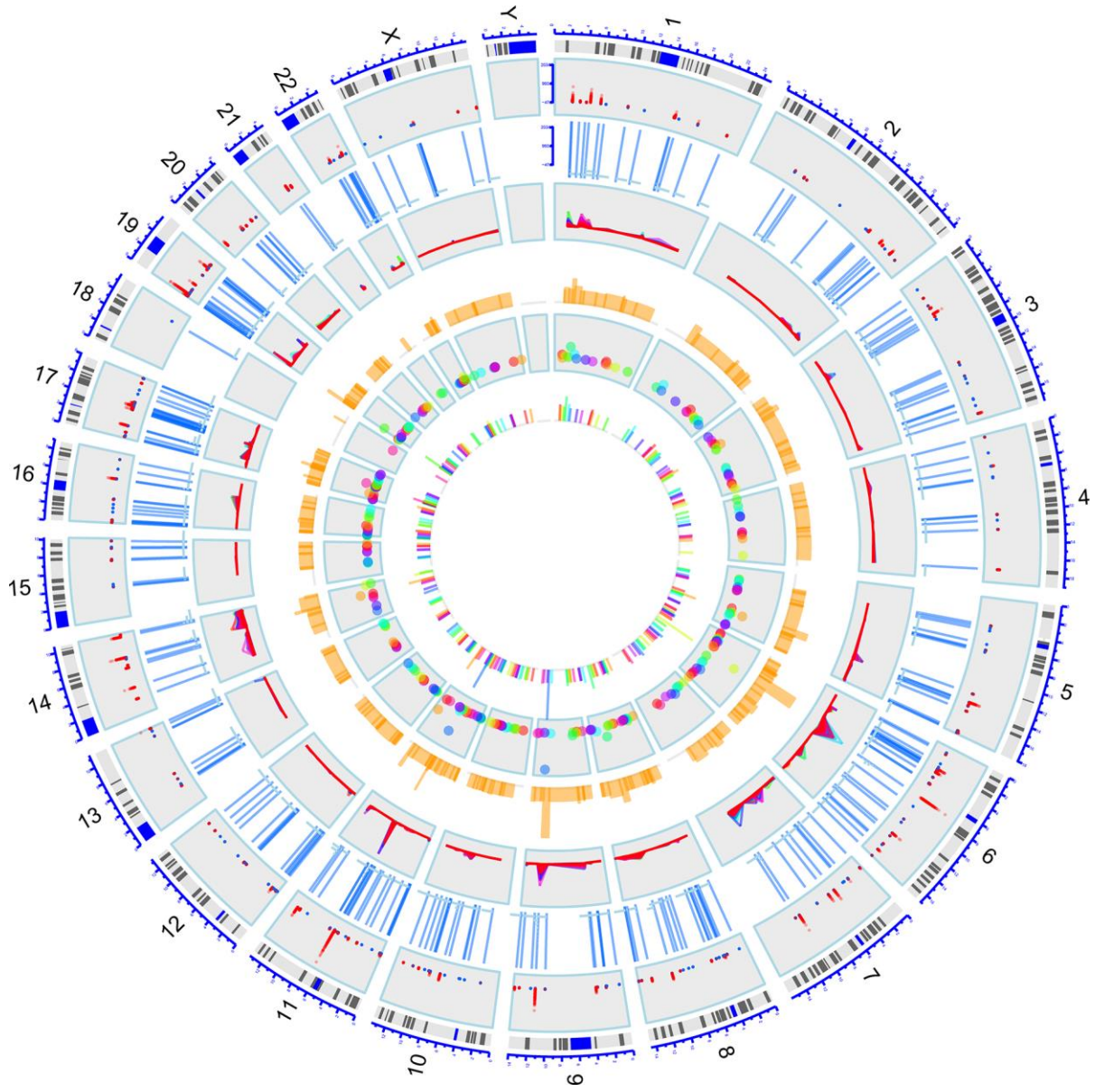

Supplementary Figure 1. Distribution of the DEAGs on chromosomes. A total of 307 human AGs obtained from HAGR were distributing on all chromosomes, except sex chromosome Y.

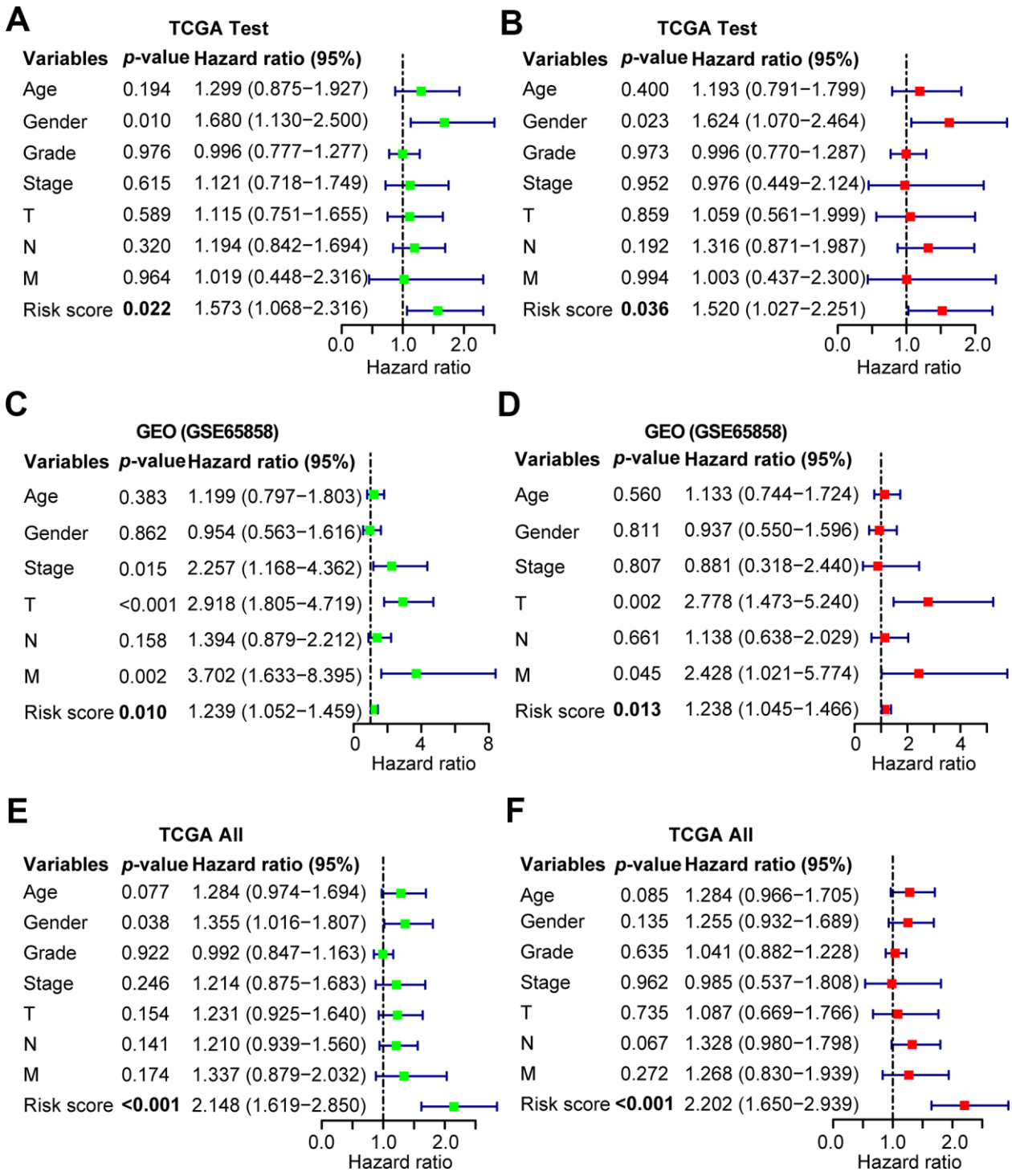

Supplementary Figure 2. Univariate and multivariate cox regression analyses of OS in HNSCC patients with other data sets. (**A**, **B**) Clinicopathological parameters of the patients in the TCGA test set using univariate and multivariate Cox regression analyses, respectively. (**C**, **D**) Clinicopathological parameters of the patients in the GEO (GSE65858) data set using univariate and multivariate Cox regression analyses, respectively. (**E, F**) Clinicopathological parameters of the patients in the TCGA all data set using univariate and multivariate Cox regression analyses.

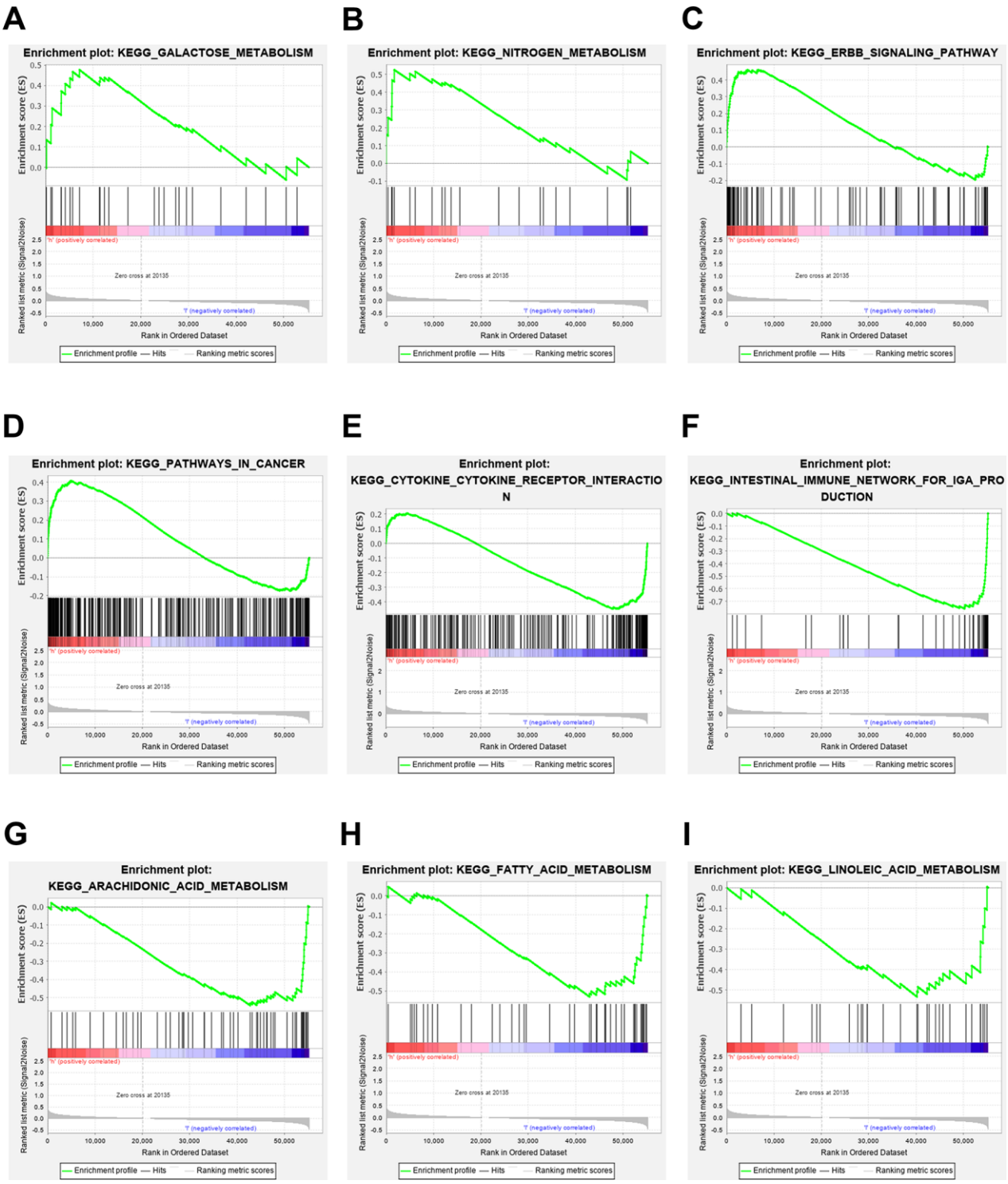

Supplementary Figure 3. Other single GSEA figures in the high-risk and low-risk groups. Single GSEA showing galactose metabolism (**A**), nitrogen metabolism (**B**), the ERBB signaling pathway (**C**), pathway in cancer (**D**), cytokine_cytokine receptor interaction (**E**), intestinal immune network for IgA production (**F**), arachidonic acid metabolism (**G**), fatty acid metabolism (**H**) and linoleic acid metabolism (**I**).

Supplementary Tables

Please browse Full Text version to see the data of Supplementary Tables 1, 3, 4.

Supplementary Table 1. Three hundred seven genes related to aging.

Supplementary Table 2. Forty-one differentially expressed genes in the aging-related gene set.

Gene	ConMean	TreatMean	logFC	*p*Value	FDR
APP	39.247603	103.3061	1.3962495	4.95E-13	9.04E-13
BAK1	10.175959	23.5007	1.2075388	1.44E-13	3.18E-13
BUB1B	3.1727858	6.922003	1.1254394	2.82E-18	1.48E-17
C1QA	27.634554	61.46906	1.1533872	0.00116444	0.001223
CCNA2	5.3256053	13.96796	1.391104	3.40E-17	1.10E-16
CDKN2A	1.3581066	10.93876	3.0097805	0.00022727	0.000258
DDIT3	5.1889558	11.92465	1.2004307	2.80E-10	3.66E-10
E2F1	2.4063142	10.09535	2.0687939	6.24E-24	2.62E-22
EGFR	9.4966372	29.37689	1.6291928	3.37E-07	3.93E-07
EGR1	177.67804	76.10728	-1.223159	3.95E-09	4.88E-09
FEN1	6.047823	19.74638	1.7071004	1.23E-22	1.73E-21
FOS	258.19873	106.0324	-1.283977	2.88E-10	3.66E-10
FOXM1	3.1564422	14.86446	2.2354956	3.97E-23	8.34E-22
H2AFX	12.914618	29.94685	1.2133993	4.93E-11	6.90E-11
HIF1A	20.036985	49.84471	1.314775	1.95E-12	3.41E-12
HMGB2	12.80035	33.52158	1.3889068	3.52E-12	5.68E-12
HOXB7	1.9075584	6.730141	1.8189094	9.78E-17	2.74E-16
HSPD1	29.136663	59.11269	1.0206322	2.16E-13	4.54E-13
IGFBP3	14.93991	52.80921	1.821618	4.89E-09	5.87E-09
IL2RG	5.2557188	10.9742	1.0621562	0.00531744	0.005447
IL7R	3.425877	8.258084	1.2693337	1.29E-11	1.86E-11
LMNB1	6.6300363	15.59522	1.234015	1.14E-11	1.71E-11
MIF	17.602226	43.2198	1.2959346	4.06E-13	8.12E-13
NRG1	2.3744663	5.626124	1.244538	7.89E-12	1.23E-11
NUDT1	5.2909544	13.01608	1.2986956	4.57E-18	2.02E-17
PCNA	24.006157	72.29586	1.5905086	4.81E-18	2.02E-17
PDGFRB	5.6199417	14.75284	1.3923654	6.67E-11	9.04E-11
PLAU	5.8109266	82.76741	3.8322227	3.61E-21	3.03E-20
PML	5.9293315	13.05956	1.139165	1.58E-14	3.89E-14
POLD1	4.3692004	9.422398	1.108725	4.68E-20	2.81E-19
PRKDC	8.5063936	19.21432	1.1755628	4.48E-13	8.56E-13
PTGS2	3.8293036	10.52787	1.4590596	0.00116031	0.001223
RAD51	2.9088248	6.234649	1.0998719	5.46E-22	5.73E-21

RECQL4	3.5042193	8.516179	1.2811132	3.91E-17	1.17E-16
SERPINE1	5.2360086	90.50704	4.1114907	3.95E-15	1.04E-14
SHC1	13.929559	33.40669	1.2619875	1.14E-17	4.33E-17
TCF3	6.2120472	14.51215	1.2241211	4.46E-21	3.12E-20
TOP2A	6.0594999	22.28673	1.8789141	2.72E-17	9.52E-17
TP63	18.548258	54.84206	1.563999	6.12E-14	1.43E-13
UCHL1	2.391086	13.05015	2.4483281	0.00077289	0.000854
VEGFA	4.337274	9.386313	1.1137699	2.10E-12	3.53E-12

Supplementary Table 3. Information for the TCGA training set.

Supplementary Table 4. Information for the TCGA test set.

Supplementary Table 5. The top thirty enriched pathways of the high and low risk scores.

NAME	SIZE	NES	ES	NOM p-val	FDR q-val
KEGG_FOCAL_ADHESION	199	1.791	0.540501	0.010	0.621
KEGG_WNT_SIGNALING_PATHWAY	150	1.787	0.467608	0.008	0.325
KEGG_PROTEIN_EXPORT	24	1.715	0.626685	0.023	0.391
KEGG_BASAL_TRANSCRIPTION_FACTORS	35	1.677	0.565968	0.028	0.391
KEGG_ADHERENS_JUNCTION	73	1.677	0.500147	0.036	0.313
KEGG_TGF_BETA_SIGNALING_PATHWAY	85	1.674	0.492573	0.020	0.267
KEGG_SMALL_CELL_LUNG_CANCER	84	1.661	0.488079	0.022	0.250
KEGG_ECM_RECEPTOR_INTERACTION	84	1.659	0.584678	0.047	0.221
KEGG_ERBB_SIGNALING_PATHWAY	87	1.658	0.460301	0.024	0.197
KEGG_RENAL_CELL_CARCINOMA	70	1.650	0.456580	0.028	0.189
KEGG_REGULATION_OF_ACTIN_CYTOSKELETON	213	1.625	0.422086	0.030	0.204
KEGG_PATHWAYS_IN_CANCER	325	1.619	0.406490	0.022	0.193
KEGG_GLYCOSAMINOGLYCAN_BIOSYNTHESIS_CHONDROITIN_SULFATE	22	1.618	0.620100	0.051	0.180
KEGG_EPITHELIAL_CELL_SIGNALING_IN_HELICOBACTER_PYLORI_INFECTION	68	1.588	0.432624	0.028	0.201
KEGG_O_GLYCAN_BIOSYNTHESIS	30	1.566	0.518195	0.047	0.214
KEGG_GAP_JUNCTION	90	1.534	0.413798	0.063	0.242
KEGG_GALACTOSE_METABOLISM	26	1.520	0.476869	0.042	0.247
KEGG_UBIQUITIN_MEDIATED_PROTEOLYSIS	134	1.512	0.414400	0.065	0.245
KEGG_NITROGEN_METABOLISM	23	1.511	0.525666	0.044	0.233
KEGG_RNA_DEGRADATION	59	1.506	0.465151	0.102	0.228
KEGG_BASAL_CELL_CARCINOMA	55	1.464	0.458399	0.079	0.272
KEGG_HEDGEHOG_SIGNALING_PATHWAY	56	1.445	0.434513	0.076	0.288
KEGG_NOD_LIKE_RECEPTOR_SIGNALING_PATHWAY	62	1.441	0.427602	0.099	0.282
KEGG_VIBRIO_CHOLERAE_INFECTION	54	1.420	0.391865	0.074	0.298
KEGG_GLIOMA	65	1.411	0.397358	0.088	0.298
KEGG_PANCREATIC_CANCER	70	1.401	0.404685	0.111	0.303
KEGG_AXON_GUIDANCE	129	1.391	0.379621	0.094	0.305
KEGG_INOSITOL_PHOSPHATE_METABOLISM	54	1.385	0.430061	0.128	0.302
KEGG_AMINOACYL_TRNA_BIOSYNTHESIS	22	1.378	0.517645	0.162	0.300
KEGG_N_GLYCAN_BIOSYNTHESIS	46	1.367	0.444909	0.128	0.305
KEGG_PRIMARY_IMMUNODEFICIENCY	35	-2.102	-0.805314	0.000	0.015
KEGG_INTESTINAL_IMMUNE_NETWORK_FOR_IGA_PRODUCTION	46	-2.047	-0.760872	0.000	0.016
KEGG_AUTOIMMUNE_THYROID_DISEASE	50	-2.021	-0.720466	0.002	0.018
KEGG_ASTHMA	28	-1.964	-0.792507	0.002	0.028
KEGG_ARACHIDONIC_ACID_METABOLISM	58	-1.916	-0.542208	0.002	0.040
KEGG_ALLOGRAFT_REJECTION	35	-1.885	-0.807991	0.004	0.046

KEGG_SYSTEMIC_LUPUS_ERYTHEMATOSUS	55	-1.813	-0.671447	0.026	0.080
KEGG_CELL_ADHESION_MOLECULES_CAMS	131	-1.797	-0.547984	0.012	0.080
KEGG_TYPE_I_DIABETES_MELLITUS	41	-1.783	-0.693100	0.028	0.081
KEGG_HEMATOPOIETIC_CELL_LINEAGE	85	-1.761	-0.568026	0.024	0.088
KEGG_NATURAL_KILLER_CELL_MEDIATED_CYTOTOXICITY	132	-1.733	-0.512719	0.016	0.103
KEGG_GRAFT_VERSUS_HOST_DISEASE	37	-1.708	-0.731792	0.047	0.115
KEGG_LEISHMANIA_INFECTION	70	-1.676	-0.553619	0.054	0.138
KEGG_FATTY_ACID_METABOLISM	42	-1.668	-0.531167	0.024	0.135
KEGG_CYTOKINE_CYTOKINE_RECEPTOR_INTERACTION	264	-1.655	-0.446398	0.033	0.139
KEGG_PARKINSONS_DISEASE	127	-1.650	-0.547933	0.053	0.134
KEGG_ANTIGEN_PROCESSING_AND_PRESENTATION	81	-1.648	-0.565163	0.064	0.127
KEGG_ALZHEIMERS_DISEASE	165	-1.641	-0.458914	0.043	0.126
KEGG_T_CELL_RECEPTOR_SIGNALING_PATHWAY	108	-1.633	-0.493802	0.042	0.126
KEGG_PEROXISOME	78	-1.621	-0.446708	0.030	0.129
KEGG_TRYPTOPHAN_METABOLISM	39	-1.612	-0.505357	0.029	0.130
KEGG_CARDIAC_MUSCLE_CONTRACTION	78	-1.610	-0.502809	0.028	0.125
KEGG_OXIDATIVE_PHOSPHORYLATION	131	-1.607	-0.542387	0.070	0.123
KEGG_B_CELL_RECEPTOR_SIGNALING_PATHWAY	75	-1.594	-0.491494	0.048	0.128
KEGG_LINOLEIC_ACID_METABOLISM	29	-1.593	-0.533346	0.045	0.124
KEGG_BUTANOATE_METABOLISM	34	-1.590	-0.503871	0.038	0.120
KEGG_ALDOSTERONE_REGULATED_SODIUM_REABSORPTION	42	-1.586	-0.471743	0.050	0.119
KEGG_CHEMOKINE_SIGNALING_PATHWAY	188	-1.564	-0.442850	0.051	0.131
KEGG_VALINE_LEUCINE_AND_ISOLEUCINE_DEGRADATION	43	-1.555	-0.524273	0.056	0.134
KEGG_FC_EPSILON_RI_SIGNALING_PATHWAY	79	-1.553	-0.432609	0.036	0.132